공학박사학위논문

Development of Systematic, Self-consistent Algorithm for the K-DEMO Steady-state Operation Scenario

핵융합실증로 정상상태 운전 시나리오를 위한
체계적이고 자기충족적인 알고리즘 개발

2017년 2월

서울대학교 대학원
에너지시스템공학부
강 지 성

Abstract

Development of Systematic, Self-consistent Algorithm for the K-DEMO Steady-state Operation Scenario

JiSung Kang
Department of Energy System Engineering
(Fusion & Plasma Engineering)
The Graduate School
Seoul National University

Korean Fusion Demonstration Reactor (K-DEMO) project is aiming to realize a net electricity generation, a self-sustained tritium, but also to be used as a component test facility. Recent progress of superconducting materials and manufacturing experiences in KSTAR magnet leads a distinct design feature of K-DEMO which is high central magnetic field at the plasma center of more than 7 T.

A burning plasma is a kind of self-organized plasma that most heating is from the alpha particle and most plasma current is sustained by self-driven current different from the present experimental device. To analyze such a complex phenomenon with a computational method, an integrated numerical package is strongly required but also a systematic and self-consistent algorithm is essential.

Based on magnet coil and its surroundings, geometrical parameters such as major/minor radius are determined. To estimate overall plasma performance, 0-D plasma operation

contour analysis code is first developed and determined a range of domain which satisfies the target fusion power in density/temperature space.

Within this calculation regime, a new algorithm for K-DEMO is developed to address a steady-state pressure and current profile under ideal magnetohydrodynamic (MHD) stability and technological level. To consider profile effect carefully which regulate plasma confinement and bootstrap current, the main variables of object function is set to be pressure and current density profile subject to the largest fusion gain. Target pressure profiles with different pedestal structures are investigated by scanning their broadness, pedestal height, and width. Formation of stable equilibria is evaluated by solving Grad-Shafranov equation and checking linear MHD stability. For the case of potentially stable equilibrium, required external heating distribution is calculated by considering both power balance and external current drive alignment to reproduce the pressure profile of the stable equilibrium. The equilibrium and corresponding external heating configuration with the highest fusion gain above target fusion power are chosen for designing an optimal scenario. As a final step, electron/ion temperature and poloidal flux evolutions are solved with the derived heating configuration to find a steady-state scenario and achieve self-consistent plasma profiles.

To implement the developed algorithm, integrated numerical package is organized with existing codes connecting with the standard data model. This code package is benchmarked with KSTAR discharge.

An economic K-DEMO steady-state target operation scenario has been studied through the designed algorithm considering self-consistency with equilibrium, stability, confinement, and heating/current drive. Steady-state solution shows a viable power plant demonstration but also produces key features of K-DEMO discharges. K-DEMO is targeting phased approach starting from the first phase of 2000 MW and the second phase of 3000 MW. Extrapolating operation regime of ITER to a high magnetic field,

2000 MW stable pressure and current profiles are derived. Additionally, assuming enhanced density limit and pedestal pressure, ultimate 3000 MW case is shown.

In conclusion, a systematic, self-consistent algorithm to find a burning plasma operation scenario has been developed for the steady-state pressure and current profile maximizing the fusion gain and applied to K-DEMO. An efficient and stable burning plasma operation in K-DEMO seems to have a good prospect in terms of current physics/engineering level.

Keywords: Nuclear Fusion, Korean Demonstration Fusion Reactor (K-DEMO), Steady-state Pressure and Current, Self-consistent Algorithm, Integrated Modelling
Student Number: 2011-30284

Table of Contents

List of Figures

List of Tables

Chapter 1. Introduction

1.1. Korean Demonstration Fusion Reactor

Korean fusion energy development promotion law (FEDPL) was launched in 2007, first time in the world, to secure fusion energy as a sustainable green energy source. The commercialization of Korea's fusion energy by the Promotion Act has a development roadmap leading to KSTAR, ITER, and Korean Dmonstration fusion reactor (K-DEMO). The goal is to procure advanced nuclear fusion device manufacturing technology through KSTAR and ITER, to develop nuclear fusion engineering technology, and acquire the ability to design K-DEMO. Ultimately, the K-DEMO construction and operation will provide original technologies for the commercialization of fusion energy.

As a part of the whole project, the K-DEMO conceptual design study [1] has been also initiated in 2012 to not only explore the pre-design parameters and operational capability but also identify R&D directions for the K-DEMO engineering design phase. The Main missions of K-DEMO are to demonstrate electricity generation and self-sustained tritium cycle while operating as a component test facility as well.

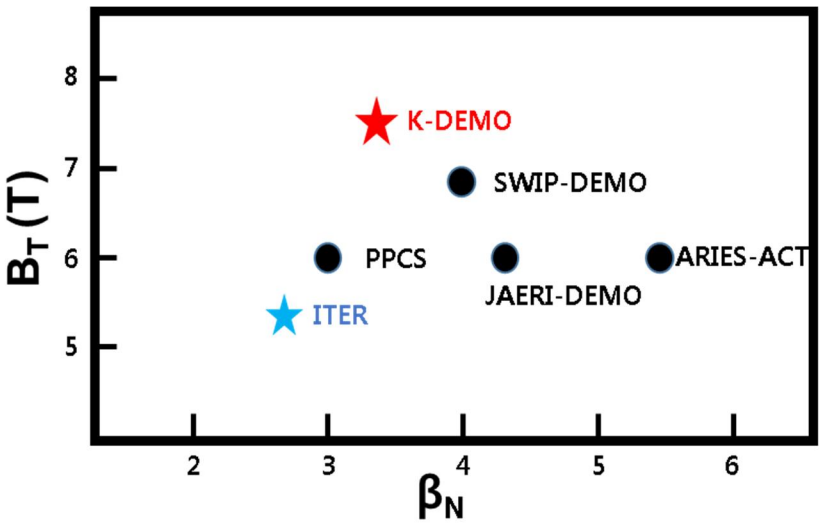

Figure 1.1. Normalized beta and toroidal magnetic field of ITER and various demo devices (K-DEMO, ARIES-ACT, PPCS, JAERI-DEMO, and SWIP-DEMO).

Generally, characteristics of demo devices could be classified by normalized beta and magnitude of toroidal magnetic field as major parameters required for the performance as shown in Fig. 1.1. A distinct feature of K-DEMO is higher magnetic field compared to other worldwide demo devices. The K-DEMO plasmas at this high magnetic field regime are expected to lead to the level of fusion demonstration power even with an ITER-size machine while other demo studies such as ARIES-ACT, PPCS, JAERI-DEMO, and SWIP-DEMO pursue a higher normalized beta or a larger major radius with a lower magnetic field [2-6]. Table 1.1 shows K-DEMO specific design parameters. Blanket 3-D view, stress analysis, coil fabvrication, divertor sketch, and overall K-DEMO sketch corresponding to parameters are in Fig. 1.2. Tungsten mono-block divertor, RAFM cooling tube, and high pressure water-cooling are used. Ceramic pebble type breeder blanket with high pressure water cooling are planned.

Table 1.1 K-DEMO Design Parameters

Variables	*Values*
Major Radius (R)	**6.8 m**
Minor Radius (a)	**2.1 m**
Toroidal Magnetic Field	**7.4 T**
Elongation / Triangularity	**2.0 / 0.6**
β_N	**< 4**
Fusion Power (P_F)	**2000 MW (1^{st}) 3000 MW (2^{nd})**
Fusion Gain	**20**
Divertor Operation	**Double-null**

To realize near-term implementation of K-DEMO, high field operation with a central toroidal magnetic field of more than 7.4 T, achievable with the present Nb_3Sn superconducor [7], is adopted as a main feature of this device. High field operation is a simple way to achieve demo-level plasma pressures without increasing normalized beta or plasma current significantly. Thermal fusion powers from 2000 MW to 3000 MW are aimed with a fusion gain of 20. Assuming successful operation of ITER, machine size (R/a = 6.8/2.1 m) and aspect ratio (A = 3.23) are set to be similar to those of ITER to utilize its construction and engineering know-hows. To align with the databases accumulated from KSTAR and ITER operations, plasma shape parameters (κ = 2.0, δ = 0.6) and normalized beta of less than 4 are chosen as constraints.

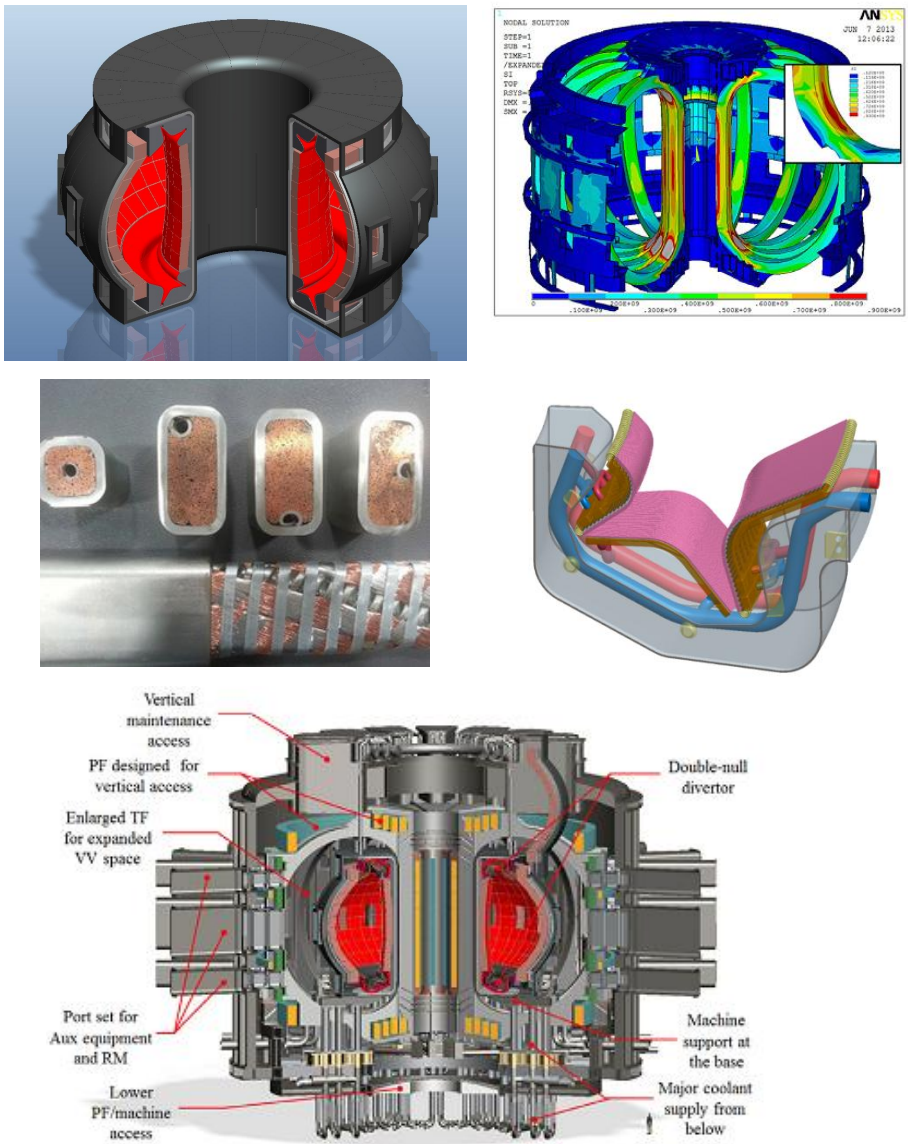

Figure 1.2. Blanket 3-D view, Stress Analysis, Coil Fabrication, Divertor Sketch, and Overall Sketch [1]

1.2. Previous Work

1.2.1. Operation Scenario Studies in Burning Plasmas

The key to efficient burning plasma operation is the self-heating by alpha particles and the ratio of self-current to drive plasma of several tens MA. An actual driving scenario is the ultimate goal of maximizing both of the above effects at the same time while achieving the maximum possible output stably. However, most of existing demo reactor operation scenarios suggest some ways to satisfy the target output and operation efficiency. Overall results are mainly on target performance reproduction. There is not a comprehensive systematic algorithm or methodology.

In this section, I summarize the problems of the driving scenario research in the recent cases, and make it possible to use it to derive the direction of this thesis.

A more specific example is the results of European demo case [4]. PPCS case (Fig. 1.3.) is a kind of trial and errors. The electron and ion temperature distributions and current density distributions in this scenario are shown in the Fig. 1.3. A self-consistent solution has been derived, but the process is not systematic.

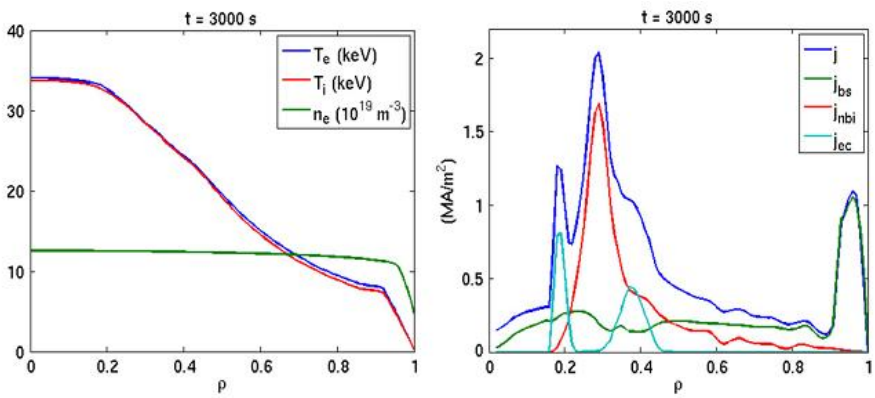

Figure 1.3. PPCS Cronos Analysis Results. [4]

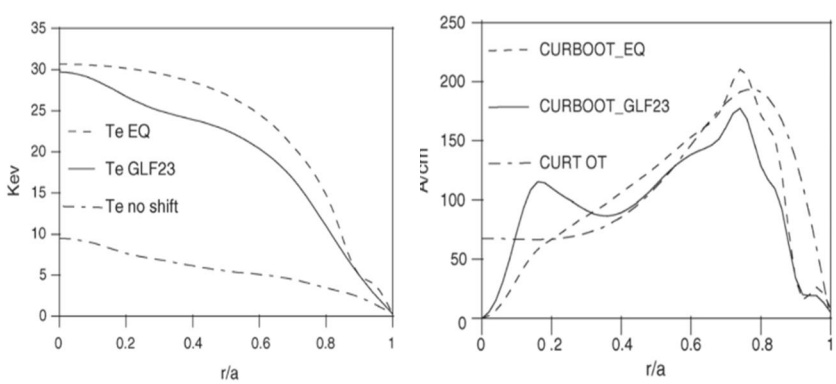

Figure 1.4. ARIES-AT pressure and current distribution [8]

In ARIES [8] case, they performed a scan that maximized the self-current ratio while changing the pressure distribution and plasma shape. derived a self-consistent one-dimensional pressure and current distribution.

Investigation of plasma profile maximizing bootstrap current fraction are also conducted [9]. Varying pressure profiles, a sequence of pressure profiles is determined in Fig. 1.4.

Major constraints are ballooning instability. The maximum bootstrap current condition obtaining process is in Fig. 1.4. It does not contain confinement physics detail.

The main optimization formula is

$$f(p) = \max\{\text{bootstrap}\} \tag{1.1}$$

where pressure profile is

$$p(\psi) = p_0[c1\left(1 - \acute{\psi}^{b1}\right)^{a1}$$

Pressure profile exploration is stopped when the bootstrap fraction reaches the ballooning boundary as the shape of the pressure changes.

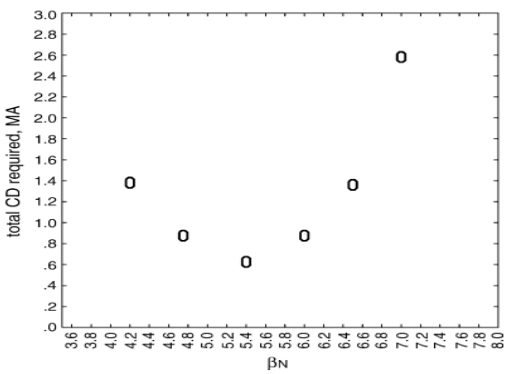

Figure 1.5. ARIES pressure profile optimization process [9].

A high beta value creates an excessive bootstrap current, rather than increasing the amount of external current drive. On the other hand, at low beta values, the bootstrap current is insufficient and the current that must be driven externally is large. For the above two reasons, the pressure distribution with the highest self-current ratio, but lower than the stability limit, is chosen.

1.2.2. Previous K-DEMO Current Density Profile Exploration

One-dimensional current density profile for K-DEMO was addressed by scanning control knobs such as injection location, beam number, and beam power assuming stable equilibria to satisfy power balance with a given transport model shown in Fig.1.6 [10]. Given one-dimensional plasma safety factor profile was cross-checked with equilibrium, bootstrap current analysis, and thermal transport analysis. A self-consistent modeling with prescribed heating schemes which is not systematic approach.

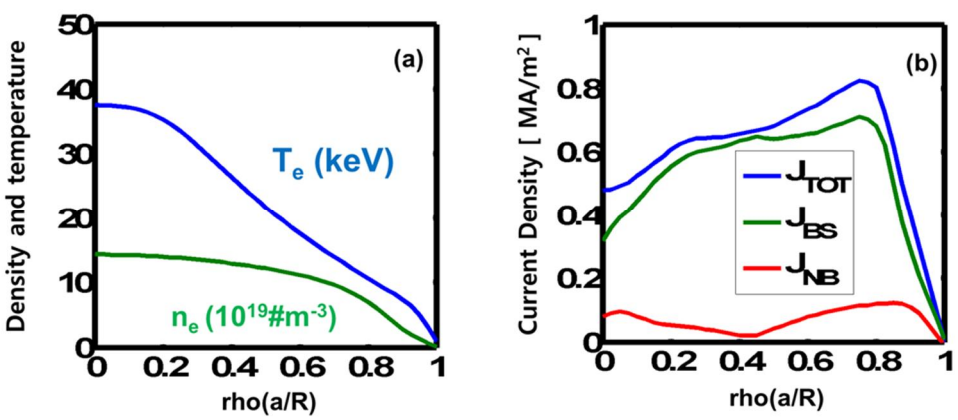

Figure 1.6. Previous K-DEMO (a) pressure and (b) current profiles.

By varying external neutral beam heating configuration, relevant conditions are classified. Scanning parameters are beam power, position, width, height, and beam number. Since broad current drive characteristics of NB, a 5% uncertainty of aligning current density profile is assumed. Variations of heating profile lead pressure profile differences with thermal transport. Pressure profile modification also makes total current density profile and bootstrap profile changes. Eventually, the amount of required external heating is changed. Those three steps are iterated equally. The lowest external heating power satisfying thermal power balance and 100% non-inductive current fraction is selected after the iteration process.

The NB injection is representatively selected in this study for external current drive method. The beam energy is set to be 1MeV to reflect the ITER specification.

The heat transport is solved by using two kinds of anomalous transport models in addition to the neoclassical contribution [11]. One is theory-based transport model, the Weiland model [12] and the other is ITER ITB diffusivity model [2]. Weiland model is based on the ITG/TEM (Trapped Electron Mode) theory, applied in various devices. [13, 14] On the other hand the ITER model would be the technological level at the ITER steady-state phase. The particle transport is not solved in this work for simplicity. Alpha particle density profile and relative

magnitude are from ITER weak-shear scenario values. [2] The boundary condition is given at rho = 0.94 assuming the constant pedestal. The toroidal rotation is assumed to be zero and the poloidal rotation is solved using a neoclassical model [15]. Z_{eff} is assumed to be 1.6 with a flat profile. The bremsstrahlung and the synchrotron radiation are considered.

Steady-state current density profile is derived within 5% margin of calculation uncertainty. Overall density slope is modified to maximize self-driven current by benchmarking ARIES density profiles [9]. As a result, such a high performance profile shown in Fig. 1.6, HH_{98} = 1.42 and P_{fus} = 2000 MW, is deduced even with the ITER level β_N = 2.8. Total plasma current of 12MA and bootstrap current of 10.5MA are achieved, showing 87.5% bootstrap fraction. The self-driven current contributes overall current density profile formation. Neutral beam configuration is optimized by adjusting total current profile and thermal power balance. On-axis and off-axis neutral beam are injected to drive current. Two beams, with a total power of 80MW, are launched: 60MW to core and 20MW to the outboard region. Since most plasma heating is by alpha heating for the K-DEMO level fusion power, role of neutral beam heating is concentrated to current drive. Finally, fusion power multiplication factor Q=25 is accomplished with this external heating configuration.

1.3. Research Objective

The main purpose of this dissertation is to develop a new systematic, self-consistent algorithm to predict an optimum current density and pressure distribution for the K-DEMO steady-state discharge. Previous studies suggest that a certain scenario can be obtained but does not guarantee a comprehensive optimization of performance for the given device. PPCS just suggests some pressure and current profiles to satisfy the target output. ARIES scenario was developed only by maximizing bootstrap current for different pressure profiles, resulting in optimum beta normal value instead of maximum beta, or changes the plasma shaping individually to enhance the stability of the plasma. They could not consider energy confinement optimization process. The previous K-DEMO scenario study successfully obtained an optimal pressure and current density distribution to meet both power balance and fully non-inductive current drive by scanning the external heating configuration. However, only for a given safety factor profile without a systematic algorithm are considered with prescribed heating combinations.

In this thesis, a new systematic, self-consistent algorithm containing confinement,

stability, and heating/current drive requirements is developed to find a steady-state pressure and current profile with maximum fusion power gain. The new algorithm presents stable target pressure and current density distributions and systematically finds corresponding self-consistent external heating configurations.

The contents of the thesis consist of the development of numerical package to analyze burning plasmas, the development of new optimization algorithms, and finally derivation of the K-DEMO operation scenario with these developments.

Chapter 2 discusses the development and acquisition of computer simulation tools. A 0-D system analysis code is developed to analyze overall plasma performance and derive an operation domain in density/temperature space. Various numerical codes covering equilibrium, transport, stability, heating and current drive are integrated to describe self-consistent burning plasma phenomena. A standard data model and unified framework connect these numerical tools.

Chapter 3 explains the optimization algorithm maximizing fusion gain, which is not analyzed simultaneously in the previous research. A systematic, self-consistent algorithm is developed to find pressure and current profiles and corresponding heating/current drive specification containing confinement, stability, and heating/current drive requirement.

Finally, in Chapter 4, the algorithm is implemented in the established numerical

package, and the optimal pressure and current density distributions for K-DEMO steady-state operation are derived.

Chapter 2. Numerical Apparatus

An integrated numerical package named as Korean system-code is prepared to deduce the K-Demo parameters and current drive configurations where multi-dimensional codes from 0d to 2d are incorporated. The conceptual design variables, operation regime, and current drive configurations are primary calculation results.

Requirement of an integrated modeling

Figure 2.1. Physical picture of burning plasma pressure and current self-organization.

Burning plasma has self-heating properties by the alpha and self-driven current by the bootstrap current generated by the pressure gradient in the toroidal structure. The pressure and current distributions are strongly coupled as shown in Fig. 2.1. One-dimensional profile effects must be considered to take into account the most important alpha particle heating and self-current.

In order to predict and interpret the behavior of such a plasma, a multi-dimensional integrated analysis system capable of interpreting major physical phenomena comprehensively is indispensable.

2.1. 0-D System Analysis Code

2.1.1. Plasma Operation Contour Analysis

Theoretical analysis and analysis through computer simulation must precede actual device design. In the field of nuclear fusion, it is being studied through this method, and it is carried out through various methods such as MHD method and gyrokinetic method. Among them, the tokamak system analysis code is a zero dimensional simulation method that calculates the physical and engineering parameters of a fusion reactor under the basic conditions such as the heat output to the fusion and the composition of each component material. The empirical formulas based on the fusion theory and the large tokamak experiments accumulated over the past half century are included as the mean or peaking factor of each plasma parameter and these equations are used as optimization points (Building Cost, Operation Cost, Fusion Power Gain factor, etc.) to find a solution.

With zero-dimensional system code, operation regime analyses are performed to find a proper operation density and temperature in the aspect of the global thermal power balance.

Figure 2.2. shows an operation regime scanning process with physics constraints in K-DEMO. The Greenwald density [16] fraction and the normalized

beta limits draw boundary lines in the density temperature space, and minimally required fusion power sets the other calculation boundary which is presented with the dashed black circle in Fig. 2.2. The global power balance equation is solved to select the operation density and temperature regime with the lowest external heating power. The NB current drive power is assumed to be the only external heating power in this analysis.

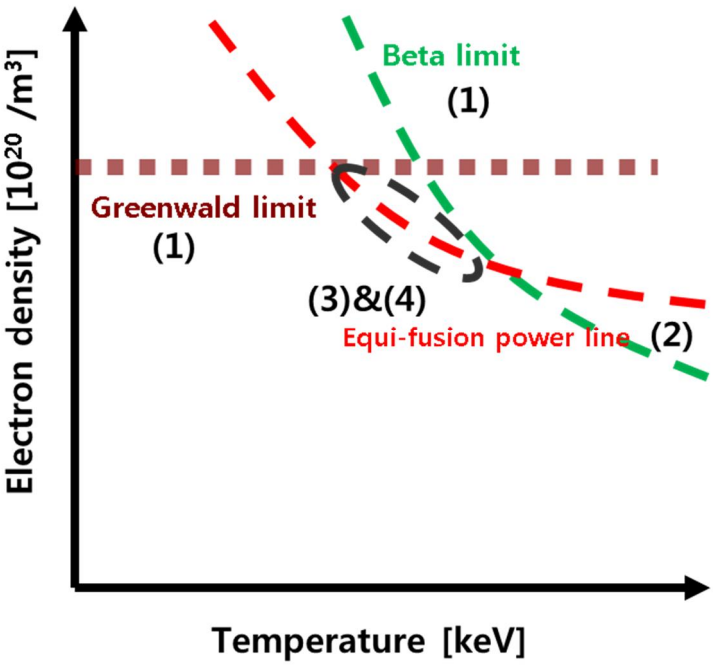

Figure. 2.2. Procedure of determining the K-DEMO operation regime

(1) Draw density and temperature limit
(2) Determine target fusion power line
(3) Solve power balance equation
(4) Select density & temperature with the lowest P_{ext}.
Slightly improved exploration procedure from W. A. Houlberg's work [17].

2.1.2. 0-D Formulation

Tokamak geometrical parameters are defined in Fig. 2.3. These parameters such as major radius, minor radius, aspect ratio, elongation, and triangularity not only define tokamak plasma geometry but also influence tokamak performance and even operating regimes.

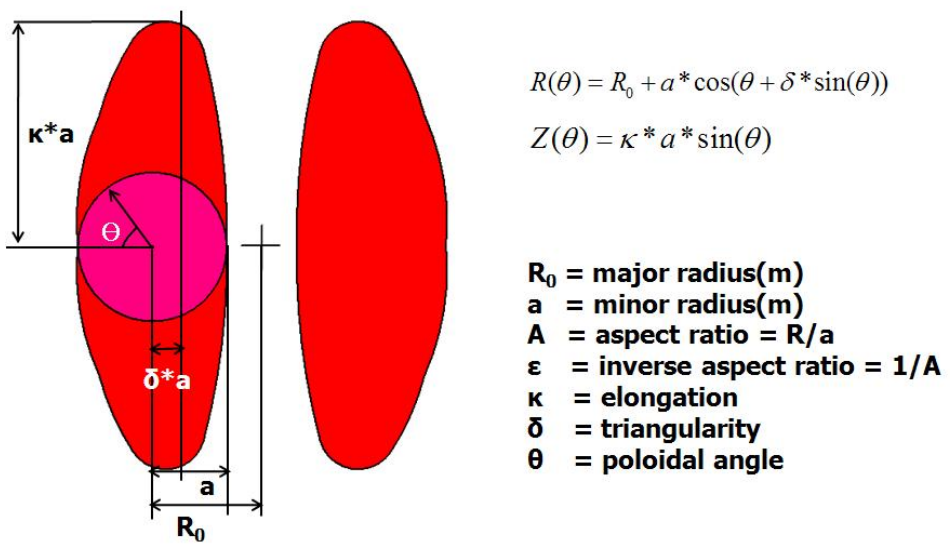

Figure 2.3. Tokamak geometrical parameters.

Maximum achievable elongation within vertical stability limit can be expressed as a function of inverse aspect ratio as following [18]

$$\kappa_{\max} = 1.46155 + 4.13281\varepsilon - 2.57812\varepsilon^2 + 1.41016\varepsilon^3 \tag{2.1}$$

Plasma volume and surface area can be calculated with the elongation. Triangularity is not accounted in this model.

$$V_P = 2\pi^2 a^2 \kappa R$$

$$S_P = 4\pi(Major\_radius + Minor\_radius + Scrape\_off\_layer)^2 \tag{2.2}$$

Higher safety factor usually guarantees better stability and minimum safety factor is limited by frequent occurrences of major disruptions. Safety factor value can be calculated approximately [19]

$$q = \frac{1}{2\pi}\oint \frac{1}{R}\frac{B_\Phi}{B_p} ds \tag{2.3}$$

When q profile calculation is considered, [12]

$$q = \frac{5a^2 B_T}{I_P R_0}\left[\frac{1+\kappa^2}{2}\right] \tag{2.4}$$

According to Wong the minimum safety factor is a function of aspect ratio as following; [20]

$$q_{\min} = 1.21 + 1.3A - 0.25A^2 \qquad (2.5)$$

Then, available maximum plasma current is limited by minimum safety factor for given major radius, minor radius, elongation and magnetic field on axis, i.e.

$$I_p = \frac{5a^2 B_0}{R_0 q_a} \frac{(1+\kappa^2)}{2} \qquad (2.6)$$

Plasma beta is ratio of plasma pressure and magnetic pressure. Wong described normalized beta limit with aspect ratio, elongation, and pressure peaking factor

$$\beta \leq C_T \left(\frac{I_P}{aB_0} \right)$$

under Troyon beta limit.

(2.7)

The Wong normalized beta limit is [20]

$$\beta_N + \beta_{N\_\alpha} + \beta_{N\_NBI} \le \beta_{N\_\max}$$

$$\beta_{N\_\max}(A) = \frac{\left(3.09 + \frac{3.35}{A} + \frac{3.87}{A^{1/2}}\right)\left(\frac{\kappa}{3}\right)^{1/2}}{100 * Peakfactor^{1/2}} \qquad (2.8)$$

Poloidal beta and toroidal beta is [21]

$$\beta_T = \frac{I_P A \beta_N}{R_0 B_T}, \beta_P = \frac{2\beta_T q_{cyl}^2 A^2}{(1+\kappa^2)} \qquad (2.9)$$

Temperature and density spatial distribution are assumed to have parabolic profile.

Then, these terms are expressed

$$n(r) = n_0\left[1 - \left(\frac{r}{a}\right)^2\right]^{\alpha_n}$$

$$T(r) = T_0\left[1 - \left(\frac{r}{a}\right)^2\right]^{\alpha_T} \qquad (2.10)$$

Where T_0, N_0 is peak value.

Plasma density is related to Greenwald density limit. Maximum plasma density is

$$\overline{n} \le f_{GW} \frac{I}{\pi a^2}$$

determined by this limit.

(2.11)

When density profile is considered, volume averaged density is

$$< n_e >= \frac{\overline{n_e}}{\left(1+\frac{\alpha_n}{2}\right)} \qquad (2.12)$$

Where unit is $10^{20}m^{-3}$.

Multiplication of plasma temperature and densities are [14]

$$P = nT(1.6\times10^{-19})Joule/eV \qquad (2.13)$$

Numerically integrating temperature, density, average temperature can be

$$< T >= \left(\frac{\beta_N I_P B_T}{2R_0 \varepsilon \mu_0 < n > 1.6\times10^{-19}}\right) \qquad (2.14)$$

Where ε is inverse aspect ratio and μ0 is permittivity of vacuum.

The important issue which can magnificently decrease current drive power is bootstrap current fraction. Bootstrap fraction is a function of inverse aspect ratio

$$f_{BS} = k_{BS} * Peakfactor^{0.25} * \beta_P * \sqrt{\varepsilon}$$
$$k_{BS}(A) = 0.6783 + 0.0446/A$$

and poloidal beta. [21]

(2.14)

When non-inductive current driving neutral beam deposition profile is parabolic

$$E_b = 100 < n_{e-20} > L_b$$

$$L_b = \left[\left(R_0 + a \right)^2 - R_0^2 \right]^{1/2}$$

and tangential injection at R_0

(2.15)

where L is the beam distance to the plasma axis.

Current drive efficiency(γ_{CD}) is set to 50%.

$$P_{CD} = \frac{n_e R_0 I_P (1 - f_{BS})}{10^{20} \gamma_{CD}}$$

Therefore, current drive power is

(2.16)

Energy confinement time uses ITER the H-mode IPB98y2 scaling law [22]. This

$$\tau_E = H\tau_E^{IPB98(y,2)}, \tau_e = \tau_i = \tau_E$$
$$= H0.0562 I_P^{0.93} B_0^{0.15} (P_{con} vol)^{-0.69} \bar{n}_{19}^{0.41} M^{0.19} R_0^{1.97} (\frac{a}{R_0})^{0.58} \kappa^{0.78}$$

equation is

(2.17)

Where H is confinement enhancement factor and M is average mass number.

0-D formulation validation

Before applying to K-DEMO, the 0d analysis scheme is validated with KSTAR reference H-mode shot #16549 (Fig. 2.4.). Plasma parameters calculated with the 0d routine such as density, temperature, stored energy, and normalized beta values are

found to be

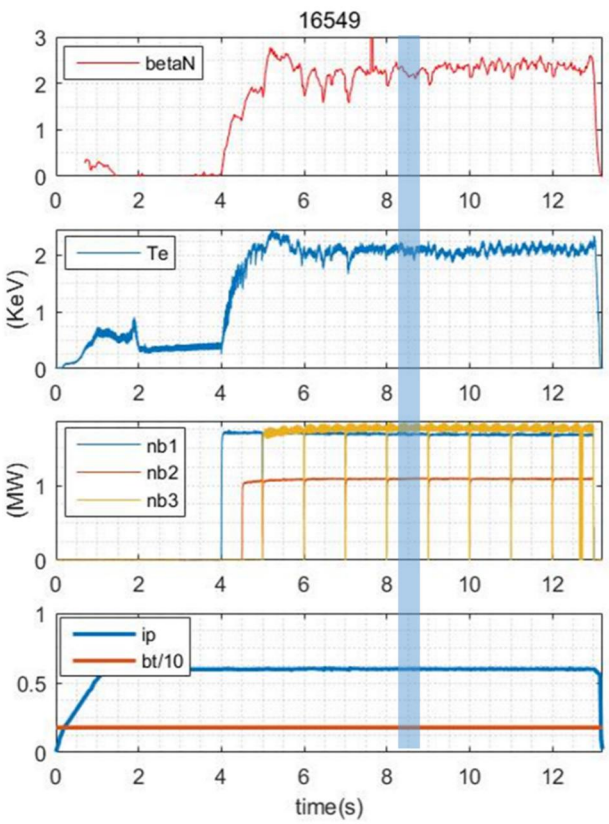

Figure 2.4. KSTAR #16549 beam driven plasma. Analysis point is highlighted with blue color.

consistent with the experimental values.

2.2. Integrated Numerical Package

A lot of numerical codes are unified with standard data model based on Fortran/Python framework. Consequently, it would lead an object-based numerical analysis.

2.2.1. Data Model

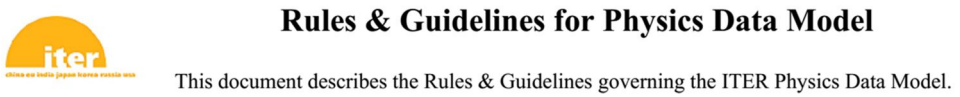

Figure 2.5. IMAS Data Model [23]

ITER integrating modelling activity developed the standard data model. [23]

The reason for selection is as follows. ITER adopts ITER data model for joint research. The structure for simultaneous use of experiments and computational simulation is available for all fusion devices as well as ITER, based on universal design rule.

To be able to describe physics and physics utilization information covering all experiments and computer simulation results. It tells the data providers and consumers what data they have, what their names are, and how they can search for users. Ultimately, the goal is to facilitate cooperation and development in various

groups.

The IMAS Data model is a kind of data structure of type Tree. (Top level -> sub structure)

Top Level: Represents physical quantities or tokamak subsystems.

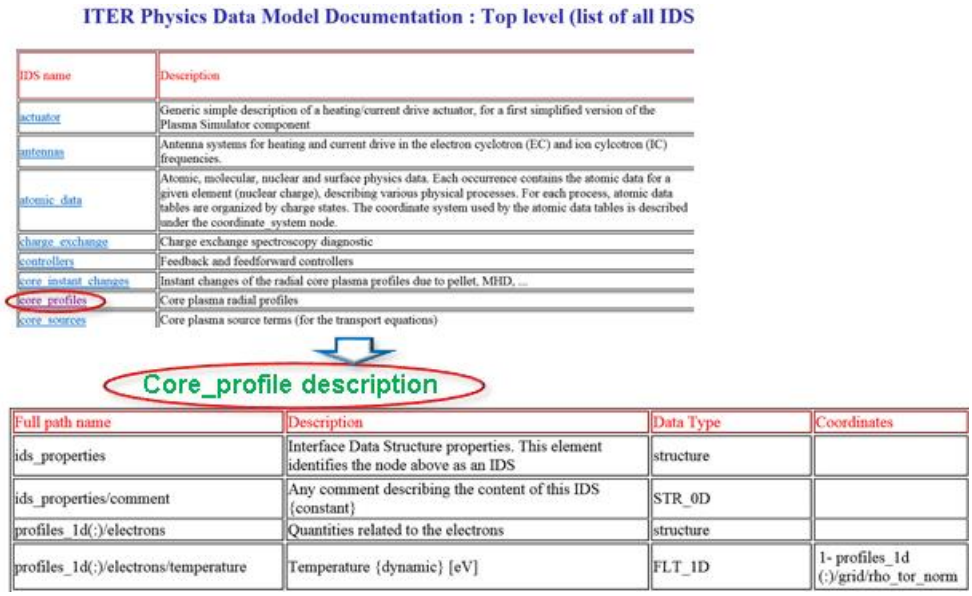

Figure 2.6. Example of data structure. [23]

Each data has its own unique path, time dimension coordinate unit, etc. and their definition is described in table 2.1.

Table 2.1. Definition of Data Structure [23]

Acronym	*Definition*
API	Application Programming Interface

CBS	CODAC Breakdown Structure, the division by CODAC of their equipment, using an EPICS conforming non-semantic naming convention
DD	Data Dictionary
DM	Data Model
IDS	Interface Data Structure. Defines the point at which a node and its children can be used in a workflow
PAPI	Physics Application Programmer Interface
PF	Poloidal Field, as in Poloidal Field system, includes all toroidally symmetric components, such as PF Coils, CS coils, and VS coils
PUAL	Physics User Access Layer, unique access to the Physics Data Model

2.2.2. Code Modules

The numerical package is composed of different modules such as 0d system analysis code, 1d transport code and 2d equilibrium & current drive codes. The list

of modules implemented is given in table 2.2. As shown in 2.1, zero dimensional system analysis code analyzes conceptual design parameters and operation regimes with physics and technological constraints. ESC [24] /CHEASE [25], a fixed boundary equilibrium code, calculates two dimensional MHD equilibria. The ASTRA code [26] is selected as a main transport solver for particle, heat, and current on each magnetic flux surface. Theory-based heat diffusion code TGLF [27] is directly linked with ASTRA. CURRAY for ICH [28] and NUBEAM [29] for neutral beam injection are utilized to the integrated simulation system to estimate the current drive efficiency and power absorption. Particle transport and plasma rotation are not considered in this study. Linear ideal magnetohydrodynamic stability calculation is conducted with DCON [30] and MISHIKA1 [31].

.

Table 2.2. List of Modules

Acronym	*Purpose*	*Details*
0D	Od analysis	0d system analysis
EQ	2D Equilibrium	Fixed boundary 2d Grad Shafranov solver

TR	1D Transport	1D Neoclassical & Anomalous transport models
WR	Geometrical Optics	IC ray & beam tracing
NB	NBI	Monte Carlo Neutral Beam driven current & power
MHD	Stability	Linear ideal MHD stability analysis

Connecting modules with framework/database

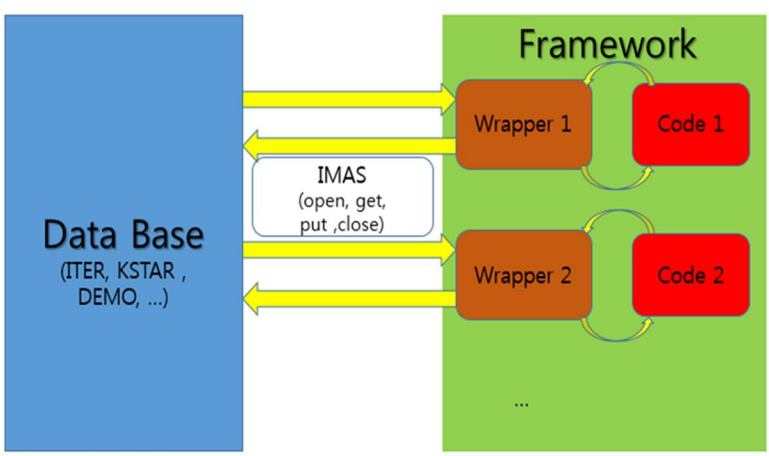

Figure 2.7. Example of code couplings

Step to integrate a module in the framework with data model could be followed shown in Fig. 2.7.

.

- ✓ Create a wrapper routines (Fortran, python, C++):
  - ✓ Prepare input file: read data from IMAS
  - ✓ Call module (stand-alone code or compile from source)
  - ✓ Read output file : update data into IMAS
- ✓ Compile the wrapper with IMAS library => stand-alone code
- ✓ Call this stand-alone code within a framework (python or fortran)

Example of source codes are in Appendix B.

The requirements of framework are as follows. A framework for K-DEMO was developed to explore loosely-coupled complex physical phenomena. Its main purpose is to provide a flexible framework and to provide a range of computational capabilities that are needed by key scientists to focus on mathematical and physics problems outside the research field and to take advantage of the answers to these challenges. Flexibility in the interchange of physical components requires standardized gathering to avoid grasping all the individual data between components required for data exchange.

Because it is intended for massive computer simulations like fusion plasma, the

framework must ultimately support everything from laptops to desktop Linux to high-end systems. Furthermore, because the resource is a scheduled resource to a batch file, the framework must invoke several independent physical operations, which must be under the load of one batch file in order to avoid latency in each operation step. It is designed to provide a framework that provides simulation identification and control into a single unified input file.

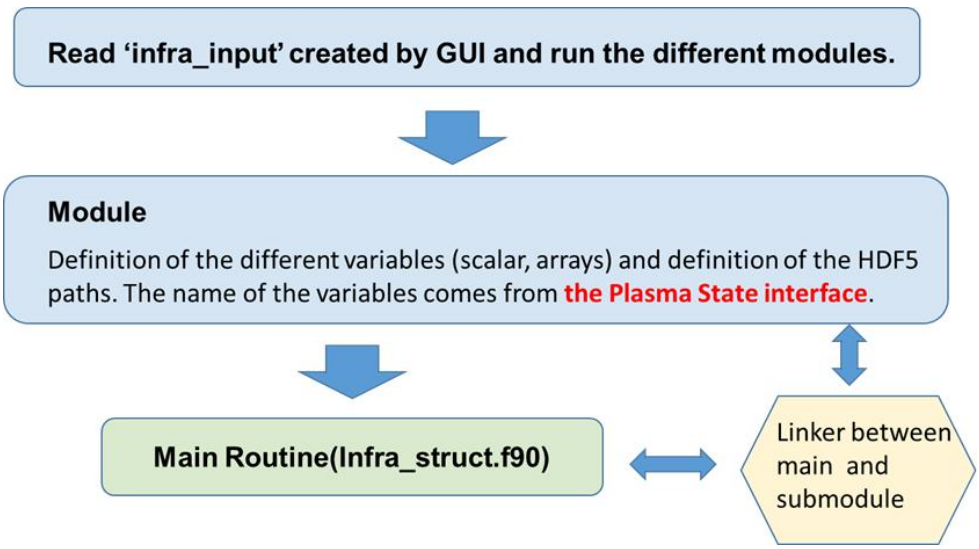

Figure 2.8. Process of each module run

Figure 2.8. shows how the actual source code is implemented. Read the infra_input file created by the GUI setting and run each module. The module defines each scalar and array value based on the value from the plasma data structure. The main routine determines the execution order of each module, and the linker connects each module.

Status of code connection

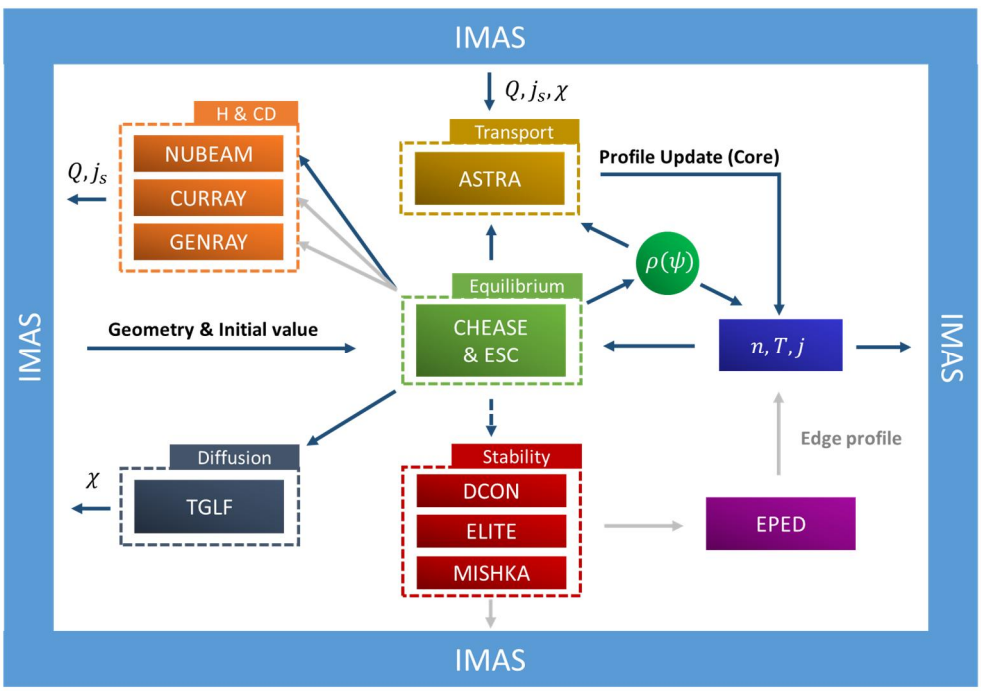

Figure 2.9. Code connecting diagram with standard data model. Connected ones are with real line, unconnected ones are with grey lines.

Figure 2.9. shows connecting structure in this system. Various codes are coupled based on modern modeling framework structure communicating with standard data model, which has flexible capability of systematic algorithm design.

By adopting the ITER data model and selection rules, a plasma data model

structure was constructed to form a standardized data bus. We modularized various codes in a Python script-based workflow engine. It is a structure that develops an optimization algorithm, weaves the modules based on it, and creates a calculation workflow during the current period to produce the result. To collect the results of several modules, we took input from the data structure at every step of the calculation and updated the output.

Key for this step is coupling transport and equilibrium. MHD equilibrium solves plasma parameters in flux coordinate and calculation domain of other codes such as transport and hearings is real geometry. So those two codes are partly directly linked to update final pressure and current distribution for each time step and update it to data base. Overall, it provides extended/flexible 1.5-dimensional integrated modeling activity. This integrated system also Accelerate repeated cycle of modeling, experimental validation, and scenario design/development. Furthermore, they Allow easy plug-in/out new codes identified important for optimization.

In the development of integrated code, a workflow based on Python is implemented as shown in Fig. 2.10. Enter start time, end time and time interval to execute and save data to data bus.

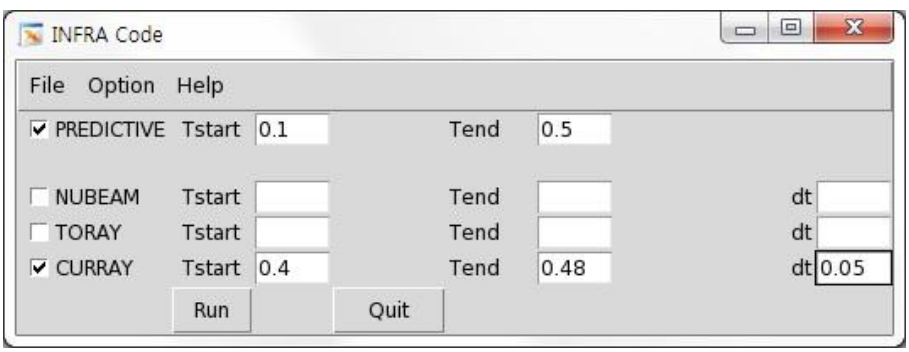

```
[lterzolo@sophie fortran]$ module avail

--------------------------- /work/imas/etc/modulefiles ---------------------------
fc2k/3.2.5                imas/master/3/ual/master
imas/3.2.0/ual/3.2.3      kepler/2.4

---------------------- /home/users/lterzolo/privatemodules/ ----------------------
kepler/2.4-clone

------------------------ /usr/share/Modules/modulefiles ------------------------
dot             module-info    mpich2-x86_64 use.own
module-cvs      modules        null

------------------------------ /etc/modulefiles ------------------------------
GCC/4.8.3               intel/15.0.3          mdsplus/stable
Intel                   java/apache-ant/1.7.1 python/2.7/15
attila                  java/jdk/1.6.0        saxon-HE/9.6.0.4
blitz/0.10              mdsplus/5
gnu                     mdsplus/alpha
[lterzolo@sophie fortran]$
```

Figure 2.10. Code run and install status

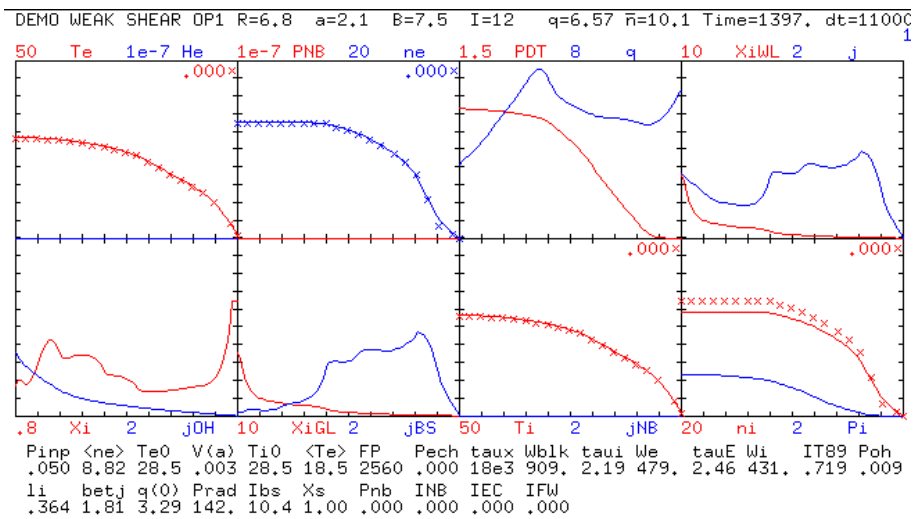

Figure 2.11. Example of transport run with ASTRA GUI.

Figure 2.11. shows part of the current drive calculation process. The main results such as the temperature density current over time are output as 0d value and 1d, and the output factor can be arbitrarily set by the user. The results are stored in real-time as a result file, and the results can be viewed according to the calculation time and the variables you want to see. Execution is possible by entering text in a Linux shell script. Here, we load the experiment file which is related to the input variable and the equation file related to the calculation order.

Chapter 3. Systematic, Self-consistent Algorithm

High performance steady state operation needs optimization of pressure and current profiles. Burning plasma algorithm must integrate various physics/engineering. A new algorithm is developed to cover complex burning plasma profile effect and support systematic approach toward steady-state K-DEMO operation. Main variables and constraints are shown in Fig. 3.1.

$$f(p, j) = \max\{Q\}$$

p : pressure profile j : current profile

Figure 3.1. Algorithm formulation and its constraints

By scanning main variables under constraints, maximum fusion gain solution is derived.

3.1. Flowchart

A distinctive scenario development algorithm subject to the largest fusion gain (Q) has been designed as shown in Fig. 3.2. It is an iterative procedure to derive a self-consistent steady-state solution of plasma profiles and corresponding H/CD configurations satisfying zero dimensional design parameters. Key plasma characteristics of demo compared to present experimental devices is self-heating/current fractions determined by the plasma profile distribution. Unlike conventional plasma predictive modelling, this algorithm estimates a required heating profile from the initial target plasma pressure/current density profiles.

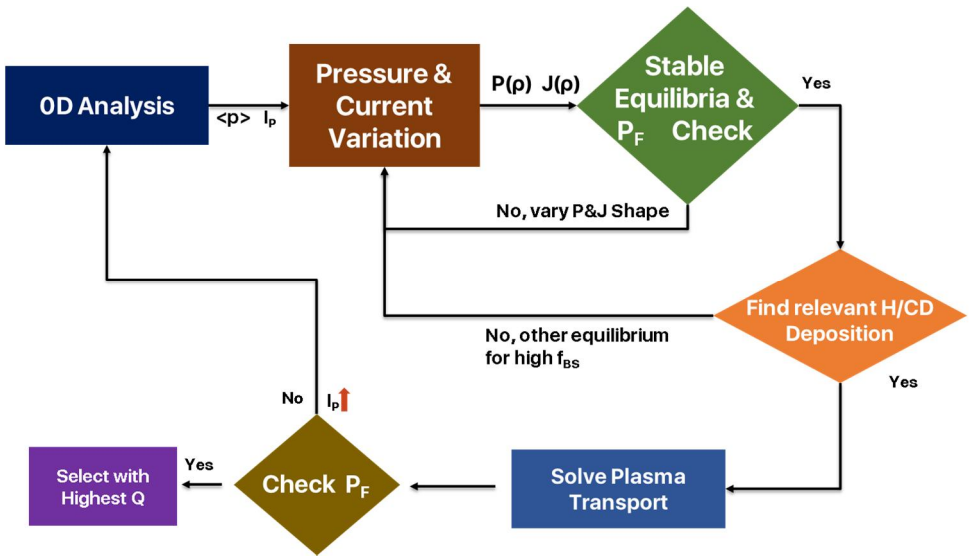

Figure 3.2. Overall Algorithm Flowchart

3.2. MHD Equilibrium and Stability

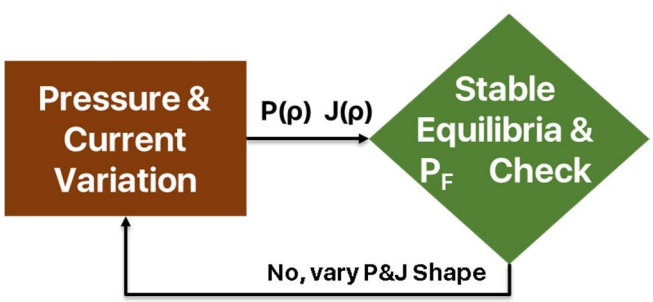

Figure 3.3. The first loop: Find stable equilibrium satisfying fusion power.

Pressure and current profiles have a significant impact on the confinement,

bootstrap current, and achievable normalized beta. Peak pressure profile is favorable for bootstrap current and broader pressure/current profile is good for confinement and stability. [32] Therefore, target profile parametrization varying peaking and broadening is essential for high performance operation.

Figure 3.4. shows exploration variables. Pressure profile with pedestal structure and current profile with two peaks are investigated. Stable equilibrium and target fusion power are evaluated scanning below coefficients in fig. 3.4. According to computation quickness, fusion power (Fig. 3.5.) and core ideal MHD stability is confirmed. Then, pedestal stability for given height is verified that its growth rate is under ideal peeling ballooning limit [33, 34]. (Fig. 3.6.)

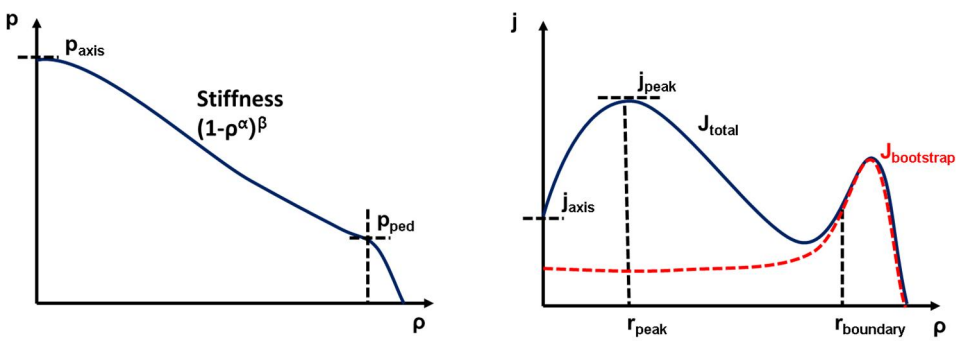

Figure 3.4. Pressure and current profile parametrization variables. Combination of coefficients are considered to investigate ITER like profiles, P_{axis} is pressure magnitude on axis and P_{ped} is value on pedestal top. Broadening between axis and pedestal is determined by α and β. J_{axis} is current density on axis and j_{peak} is on peak location (r_{peak}). Most current on pedestal is assumed to be from bootstrap current $r_{boundary}$ is the point that needs an external current drive scheme.

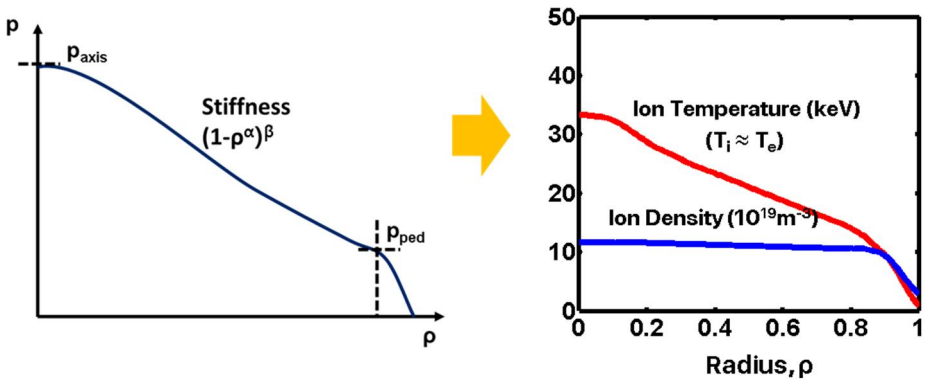

Figure 3.5 Fusion power calculation from target pressure profile. Z_{eff} Z_{imp} f_{imp} from ITER[2]. Prescribed n_e $n_{axis}/n_{ped} = 0.8$ $n_{ped}/n_{sep} = 0.3$.

If fusion power is not feasible under stability boundary, it returns target equilibrium is not achievable in this parameters and change control knobs.

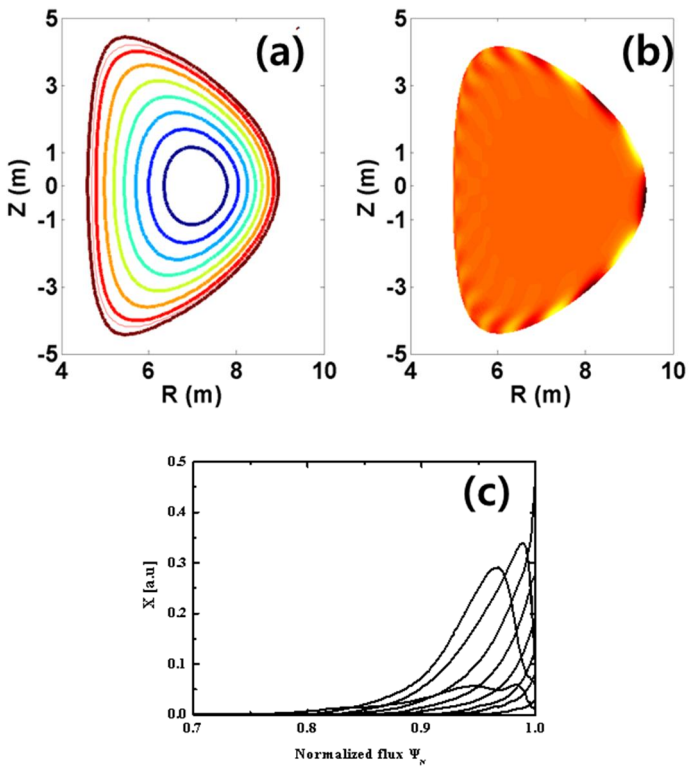

Figure 3.6. Example of stable equilibria candidate (a) flux contour (b) edge mode structure (c) n=3 mode growth rate.

3.3. Heating and Current Drive

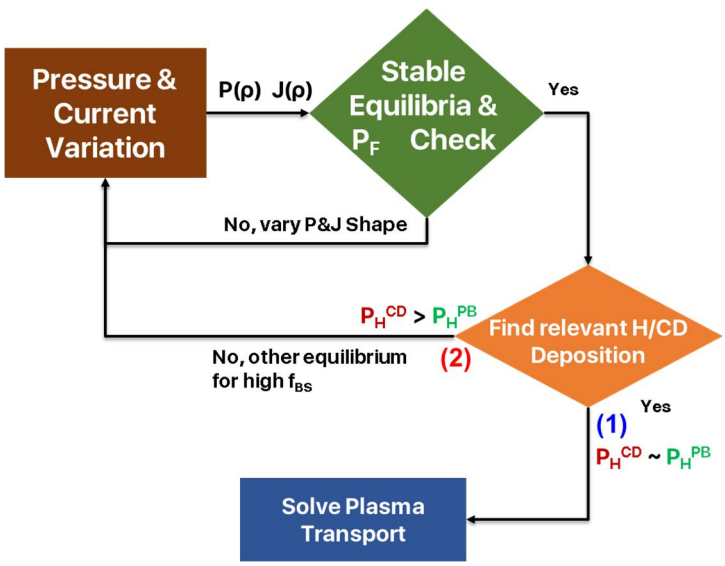

Figure 3.7. Loop 2: Derivation of relevant H/CD configuration.

Power and current balance should be satisfied for steady-state demo operation even the self-heating/current fraction for demo burning plasma is relatively lower than experimental device. Figure 3.7. shows external heating configuration determination procedure. Since heating only method like perpendicular beam injection is feasible, power scheme required for current drive is estimated in advance. Two kinds of promising external heating and current drive (H&CD) method is considered ; neutral beam (NB) and fast wave (FW). NB energy is set to

be less than 1MeV to reflect ITER NB technology and FW frequency is adjusted to avoid ion cyclotron absoprtion layers such as deutrium, tritrium, and alpha particle from out-board antenna launchear. Since magnetic field of K-DEMO is even higher than ITER, electron cyclotron heating is not examined due to its high frequency source requirement. Lower hybrid range wave system is avoided for its high density region inaccessibility.

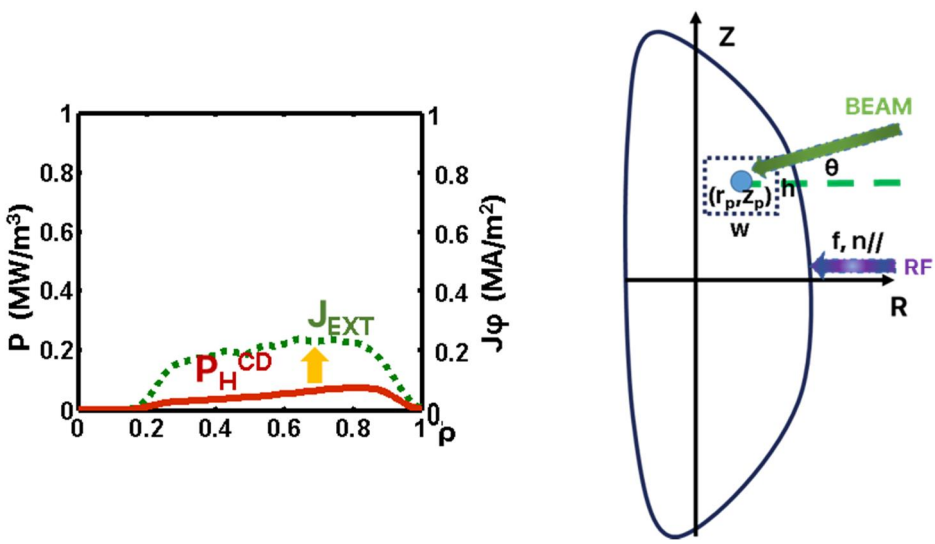

Figure 3.8. Scanning H/CD control knobs to match required external current drive.

By mixing fast wave and neutral beam injection control knobs (FW frequency/power, parallel refractive index, beam energy/power, and beam port size/location/angle) current drive profile is aligned to target distribution as shown

in Fig. 3.8. Heating from current drive (P_{HC}) is simultaneously calculated in this step.

Secondly, required external heating amount are estimated by solving one-dimensional power balance.

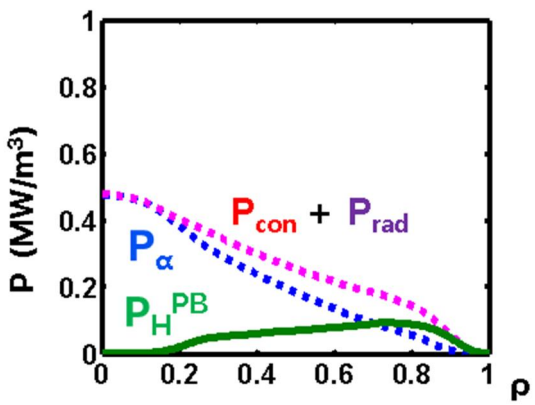

Figure 3.9. Solving 1-D power balance.

Conduction loss, radiation power, and alpha particle heating can be determined from target density and temperature distribution with diffusion models in Fig. 3.9. Required heating profile is subtracted loss power (conduction, radiation) from heating power (alpha).

$$P_H^{PB} = P_\alpha - (P_{con} + P_{rad}) \qquad (3.1.)$$

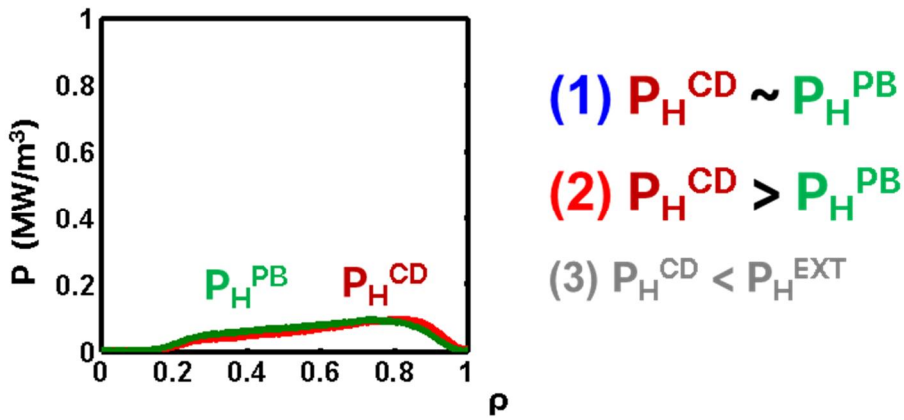

Figure 3.10. Comparison between heating from current drive and power balance.

Comparing P_H and P_{HC}, total external heating power is derived as shown in Fig. 3.10. When P_H is larger than P_{HC}, remained heating only part profile is adjusted with an additional perpendicular beam injection. While P_H is lower than P_{HC}, process would return to pressure/current parametrization step and recalculate with an increased pressure. If both two heating profiles matches well within a few percent errors, self-consistent plasma transport is solved with derived heating configuration.

3.4. Solving Plasma Transport

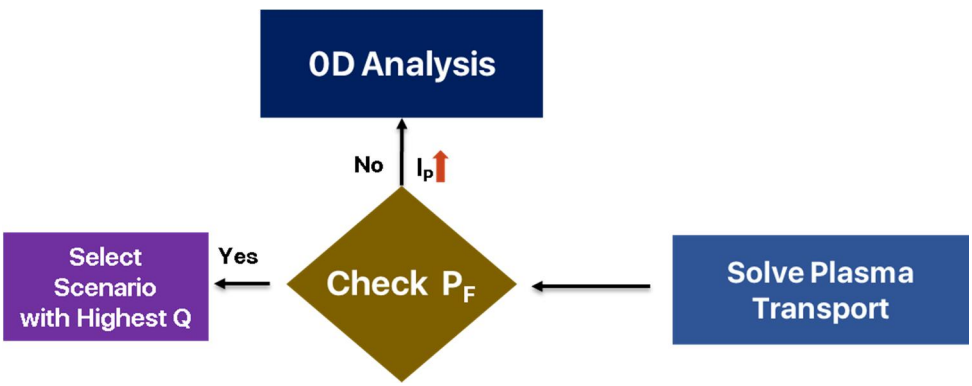

Figure 3.11. Loop 3: Check Self-consistency between Plasma Profiles and H/CD Configuration by Integrated Modelling.

Figure 3.11. is the final loop. A self-consistent plasma transport simulation with the determined H/CD configuration where the electron/ion temperature and the poloidal flux evolutions are solved to make their time derivatives zero and then its consistency is evaluated with the target 0-d performance. If the fusion power or gain is lower than the desired value, the plasma current and the pedestal height are slightly increased and fed into the algorithm again from the initial loop. As a final step, a scenario with the highest fusion gain will be selected to be the K-DEMO steady-state target scenario.

Chapter 4. Predictive Modeling of Steady-state Discharge

To apply the algorithm and numerical package on K-DEMO operation scenario, evaluation with KSTAR experiment and ITER steady-state simulation is conducted. After verifying with those things, an optimum K-DEMO steady-state pressure and current density profile is presented.

4.1. KSTAR Analysis

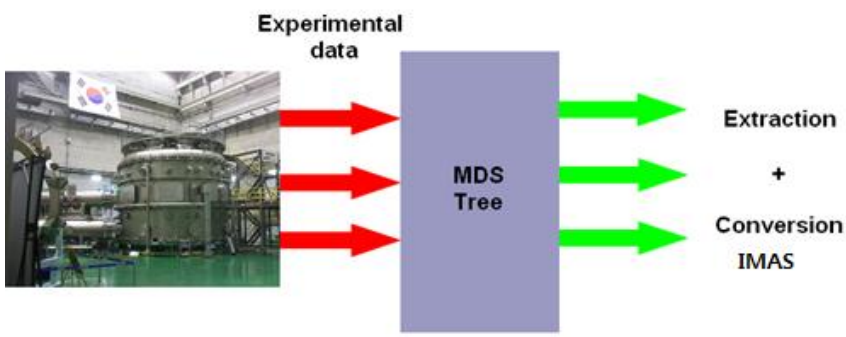

Figure 4.1. KSTAR experiment data transfer system to data base.

Sev

eral input formats have been tested to transfer KSTAR data to IMAS database such as ASCII, Ufiles, and MDSplus tree. For its direct connection from experiment data

(basic KSTAR experiment data storage system is MDS data), MDSPlus type is chosen. Density and temperature from experiment have been put into IMAS database to interpretative analysis of KSTAR discharge as shown in Fig. 4.1. For the test run of integrated code and its connection with experiment data, KSTAR H-mode beam plasma shot #16549 is investigated

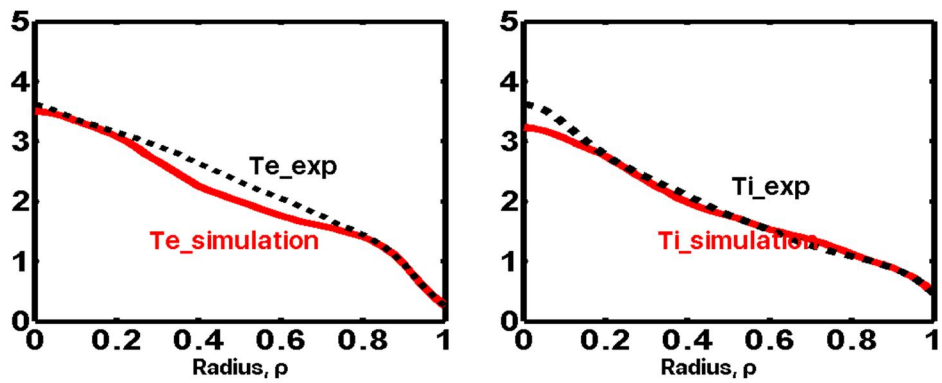

Figure 4.2. Comparison of KSTAR #16549 discharge and simulation results.

Ion and electron temperature is solved with #16549 beam configuration. (I_P = 600 kA, 5 MW NB injection) Each temperature is solved until current relaxation time. Both temperatures are mostly consistent with experimental data in Fig. 4.2. A new integrated modeling package shows good prospect for KSTAR predictive simulation.

In each case, the heat transfer coefficients of the ion and electron calculated in the

experiment and the heat transfer coefficient calculated by the TGLF model. The thermal transport coefficients of the ions and electrons calculated in the experiment and the heat transport coefficients calculated by the TGLF model have a tendency to increase outward from the center of the plasma, respectively. In this case, the heat transport coefficient of the ion is higher than the heat transport coefficient of the electron It is possible to confirm that it is big. Local experiments and model results show somewhat different trends, but overall trends or orders are similar.

TGLF model does not coincide locally with the heat transfer coefficient of the actual experiment. It can be interpreted that the experimental heat transfer coefficient is obtained by power balance analysis to obtain a given temperature gradient value, whereas TGLF can calculate mutual disparity because the given temperature gradient value is calculated as the resulting transportation coefficient.

4.2. K-DEMO Scenario

The systematic algorithm described above is applied to the K-DEMO steady-state operation scenario development.

4.2.1. Phased Approach of K-DEMO

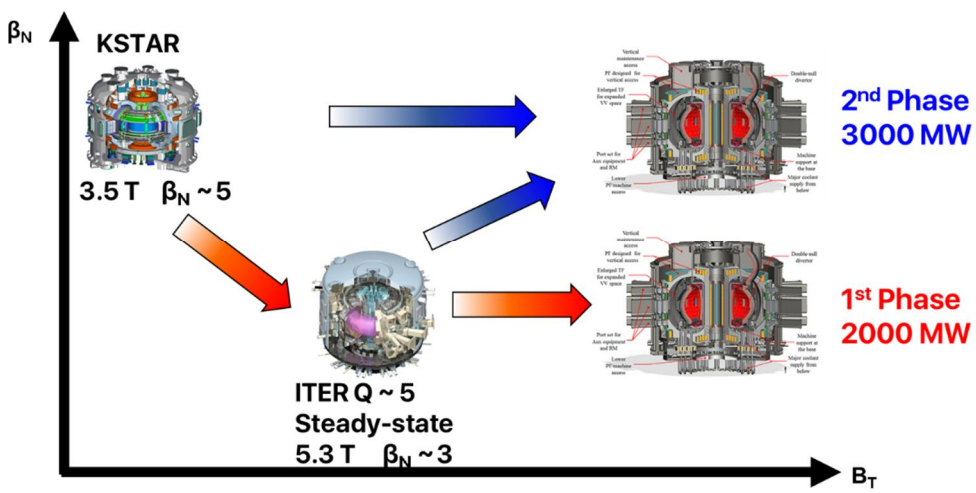

Figure 4.3. K-DEMO phased approach strategy.

The ultimate goal of K-DEMO project is a net electricity generation like other demo device concepts. Based on successful operation of KSTAR and ITER, final

goal of K-DEMO is extrapolated from them. Main idea is enlarging pressure limit and bootstrap current fraction by increasing magnetic field and normalized beta. Magnetic field represents an engineering boundary and normalized beta is for physics limit. A phased approach with respect to the fusion power is suggested as setting target fusion power values, 2000 MW at the first phase and 3000 MW for the final phase. The first phase is organized increasing magnetic field from ITER steady-state operation. After achieving the first phase, second 3000 MW is planned to combine high normalized beta experience. Ultimately, 3000 MW efficient operation is feasible.

$$\text{Pressure Limit} \propto B_T \cdot \beta_N \cdot I_P$$

$$f_{BS} \propto B_T \cdot \beta_N / I_P \qquad (4.1)$$

0d system analyzed the possibility of a phased approach. According to the results, 2000 MW and 3000 MW operation is expected from the following parameters.

- 1st Phase: 2000 MW, 13 MA, β_N - 3.2, Q - 20,
- 2nd Phase: 3000 MW, 15 MA, β_N - 3.5, Q - 25.

As in Chapter 2, emphasis is placed on the development of integrated modeling packages, zero-dimensional computations could not appropriately reflect self-driven current driven by one-dimensional profile effects. Current drive deposition has limitations in the calculation of 0d and uncertainty in current drive power prediction. Furthermore, the self-current drive forms most of the current density distribution, which greatly affects the plasma confinement and MHD stability. It is difficult to accurately predict the power distribution required in the zero-dimensional space by using Alpha heating in most of the heating power. The 3D volume effect must also be taken into account to derive the final value. In the one-dimensional distribution from the previous work, the portion occupying the largest volume is the boundary pedestal region, and the current density of this region is easy to constitute the bootstrap current. For the same reason, it is more advantageous that the value of the outboard region is larger than that of the plasma core temperature and density.

Therefore, the 0-dimensional result, like the developed Algorithm flowchart, will be the calculation domain of the multidimensional calculation. The operation scenario exploration in the next section was carried out in consideration of the multidimensional effects mentioned above.

4.2.2. Steady-state Pressure and Current Density Profiles

The systematic algorithm is applied to the K-DEMO design parameters. Various current density profiles could be explored as shown in Fig. 4.4. With pressure profiles which satisfy the target fusion power, current profile peaking variables (J_{axis} J_{peak}, and ρ_{peak}) are scanned and their overall effect is represented versus its broadness. As current profile becomes flattered, it leads to good confinement enhancement (H_{98y2}) as well as a higher bootstrap current fraction. Since plasma current is fixed in a one iteration loop, broader current profiles in the inboard region leads a wide pedestal current density profile in Fig. 4.4. When peeling-ballooning mode is unstable, broadening exploration is stopped.

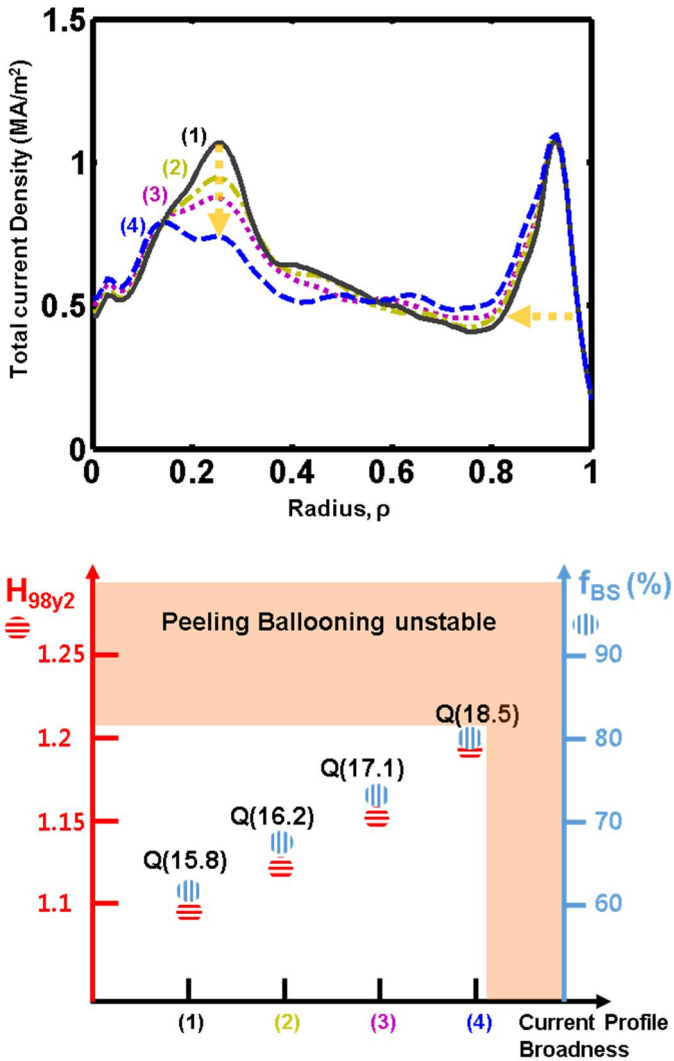

Figure 4.4. (up) Target current density profile exploration with peak height and location. (down) Confinement and bootstrap current fraction according to current profile broadness for 2000 MW target fusion power case. Left column (red) represents confinement enhancement factor and right one (blue) is for bootstrap current.

Current drive technology selection

The Korean fusion fusion is characterized by a high magnetic field, and it is possible to achieve the plasma pressure and self-current ratio necessary to obtain the fusion output and the high Q value required by the relatively low normalized beta and plasma current. However, due to the high magnetic field, technical difficulties are expected in securing the wave source like high frequency gyrotron. In the second stage of 3000 MW, it is required to have higher normalized beta and energy confinement performance than ITER. A plasma current is required.

Accessibility according to current driving method

The above-mentioned current driving method has different accessibility of the on axis and off axis depending on the type, and it becomes more important to supply the current to the necessary part because the specific current distribution is required as the operation progresses. Based on the above discussion, we set the candidate group of the current driving method of on axis and off axis as follows.

On axis candidates - IC, NB, EC

The first thing to consider when heating and driving the core plasma is the IC. In case of IC, steady state source of MW class has been developed. Neutron, thermal

shielding, and coupling problems exist. In particular, the maintenance of the integrity of the antenna should be verified in high heat and neutron environments. In the case of NB, it is the most efficient method currently used. However, in order to reach the center of the plasma at high density, 1.5 ~ 2MeV beam is required higher than the conventional 1MeV beam, and the neutron shielding and tritium contamination There are many challenges to solve. In the case of EC, development of a high frequency, power steady state gyrotron suitable for a high magnetic field is required and an increase in current drive efficiency is required. As a result, multi frequency or frequency sweeping technology should be developed for controlling the desired current drive in the environment.

Off axis candidates - NB, EC, LH, IC

In the off axis current drive, the best candidate NB is the first candidate because the IC fast wave is not suitable because it is concentrated in the center in view of accessibility. Not only does the NB have both good current drive efficiency and accessibility, but the off-axis does not require as much as ten axes of beam energy,

so the technical requirements are low, but the problem of neutron shielding remains. However, the off-axis low energy beam is very likely to be used strategically in the ramp-up phase. The EC is still less efficient than the NB, and the drift efficiency is lower due to the trapped particle effect as it goes off axis. However, gyrotron as high as ten axes is not required and is suitable for current profile control because of the advantage of local heating. LH can be used for edge plasma heating or ramp up phase because it is theoretically difficult to access the high density plasma region.

In addition, IC has recently become a possibility of off-axis current drive by high-frequency electron heating method called high frequency fast wave or helicon wave. This content is covered in more detail in the application of the latter research and development.

By this algorithm, a fully non-inductive steady-state target scenario is attained. Table 4.1. shows the results with parameters of the optimized cases and Fig. 4.5 to 4.7. present their kinetic and magnetic profiles. A phased approach with respect to the fusion power is suggested as setting target fusion power values, 2000 MW at the first phase and 3000 MW for the final phase. Starting from K-DEMO zero-dimensional parameters, the plasma current and the temperature pedestal height are increased until reaching the target fusion power under ideal peeling-ballooning stability boundary. A fusion gain of slightly less than 20 is achieved with an improved confinement enhancement factor $H_{98y2} \sim 1.2$. High magnetic field leads to those high performance parameters even with a moderate normalized beta around 3. The operation with 3000 MW fusion power was not possible with the same physics assumption as in the 2000 MW case. Therefore, by adding two kinds of physical hypothesis, the possibility of 3000 MW operation are explored. In order to obtain a high fusion output, it is advantageous that the temperature of the pedestal region occupying the most volume increases or the average density increases. Increasing the plasma current in a situation where the plasma size and the magnetic field are fixed is limited by the fact that the minimum safety factor is below 2. The minimum safety factor is set to be larger than 2 to avoid harmful 2/1 or 3/2 tearing modes. In both cases of 3000 MW, the plasma current was raised to

17 MA to ensure the maximum achievable electron density. After this, the Greenwald fraction was incrementally changed, and the algorithm was recalculated to reach 3000 MW at 110% fGW. The final case is that the Greenwald fraction was rerun and the temperature of the pedestal region was increased over the peeling-balloning stability boundary, and the possibility of 3000 MW operation was examined.

Table 4.1. Final steady-state plasma parameters

	1st phase	*2nd phase* (f_{GW} = 110%)	*2nd phase* (High T_{ped})
P_F (MW)	2070	3050	2950
Q (Fusion Gain)	19.7	23.4	22.7
I_P (MA)	15.5	17	17
f_{BS}	77 %	81 %	78 %
P_{NB} (MW)	105, 500keV	130, 650keV	130, 600keV
I_{NB} (MA)	4.0	4.2	5.2
β_N	2.8	3.2	3.1
H_{98y2}	1.2	1.17	1.17
T_{ped}	8.3 keV	8.3 keV	8.9 keV
n_{ped}	$9.9 \cdot 10^{19}$ m^{-3}	$11.2 \cdot 10^{19}$ m^{-3}	$10.9 \cdot 10^{19}$ m^{-3}

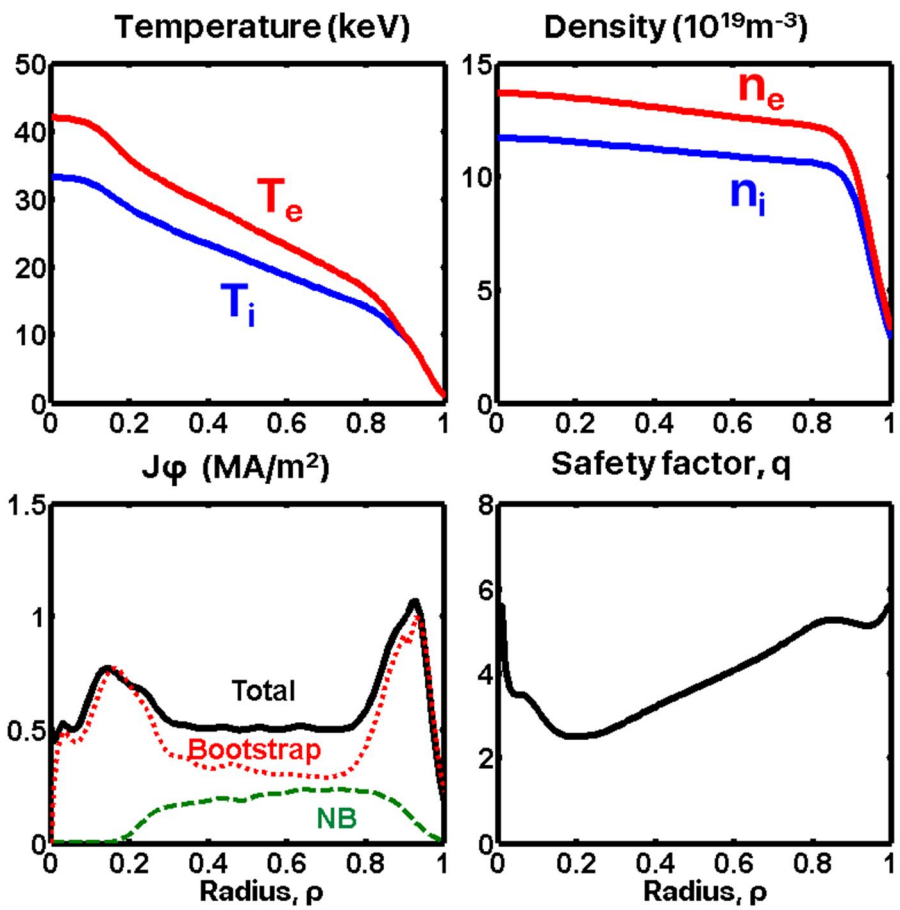

Figure 4.4. 2000 MW 1-D results.

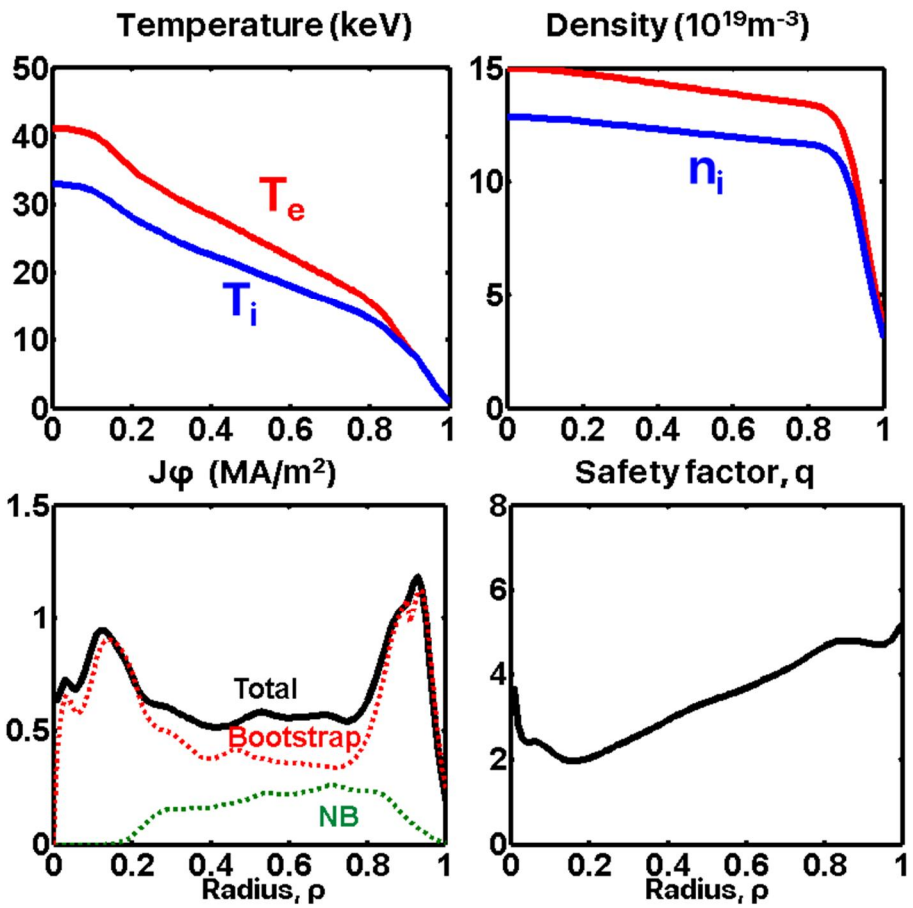

Figure 4.5. 3000 MW 1-D results with enhanced density limit.

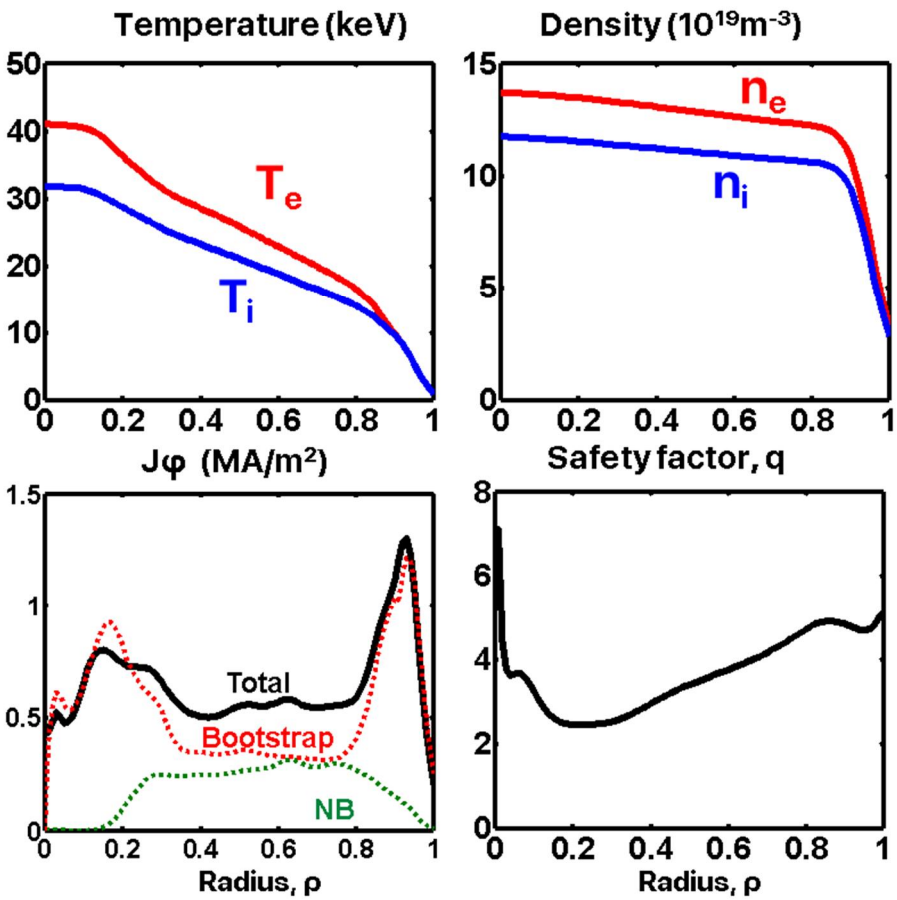

Figure 4.6. 3000 MW 1-D result with enhanced pedestal temperature.

High minimum safety factor profile scenario [35] is derived for both cases with significant bootstrap current fraction. An off-axis NBCD is used to match the external H&CD requirement. NBCD is the main control knob for external current drive method for its broad off-axis current drive capacity. The beam port location on the wall, injection angle, power, and beam energy are varied to match the target pressure/current profile. The bootstrap current tends to have two peaks on the inboard side and pedestal top where the pressure gradient rapidly changes. In this heating scheme, the off-axis beam current is mostly driven in low bootstrap dominant regions for broad current density profile which is quite consistent with DIII-D off-axis NBCD discharge [36].

Even average density is larger than ITER, optimum beam energy is around 600 keV which is about the JT-60U neutral beam energy specification [37]. Generally, higher beam energy is more effective on plasma H/CD. However, the improved confinement from current profile broadening and the bootstrap current fraction from high q_{min} are more reliable than the advantage of high energy beam injection in this demo relevant case.

Chapter 5. Conclusion

The systematic scenario optimization algorithm subject to maximize the fusion gain is newly established to develop optimal operation scenarios by integrating equilibrium, confinement, stability, and current drive requirement, self-consistently. It consists of a systematic exploration loop from zero dimensional design parameters to one dimensional transport simulation results by keeping dominant self H/CD effect of DEMO burning plasmas.

The developed algorithm and numerical package are applied to the KSTAR H-mode discharge and compared with experimental result.

For early implementation of K-DEMO, a design concept of high magnetic field operation is adopted even with ITER-size. By utilizing the integrated modeling tools and boundary conditions, a fully non-inductive steady state scenario is derived with fusion power of 2000 MW, fusion gain Q of 19.7 and normalized beta β_N of 2.8 for K-DEMO. More fusion power with efficient operation (3000 MW, Q = 23.7, 22.7) is expected by slightly increasing the plasma current (17 MA) and the stability boundary. A high q_{min} safety factor distribution ensures about 80% bootstrap current fraction without internal transport barrier. Core and edge ideal MHD stabilities are secured for the derived equilibrium.

Compared to the H&CD technology in ITER, obtained heating configurations of K-DEMO seem to be promising. Around 0.6 MeV neutral beam injection can provide a broad current profile configuration and the low recirculating power with Q greater than 20 is also encouraging. Demonstration of 100 MW beam system is a remaining technological issue.

Future Prospect

More detailed stability analysis is required for pedestal structure and plasma shaping which have a significant impact on achievable stable normalized beta. Especially, the temperature pedestal height is an important issue for this scenario. Within more reliable peeling-ballooning stability boundary, both 2000 MW and 3000 MW operation scenario would be revisited. Additional K-DEMO demonstration experiment in present experimental devices is also required by accompanying with the modeling activity. Particle transport and plasma rotation are also important for stable fusion power production and they will be updated to the systematic algorithm in the near future. Integrated time-dependent operation simulations including the ramp-up and ramp-down phase would be needed by utilizing a free-boundary equilibrium solver for full scenario development.

Appendix

A. Analytic description for 0-D power balance equation

Required external heating power for power balance could also be estimated in analytic approach. Global power balance equation could be written assuming

$$\frac{dW}{dt} = \underbrace{P_{ext} + P_{\propto}}_{\text{Source term}} - \underbrace{P_{con} - P_{rad}}_{\text{Loss term}} = 0$$

$$P_{ext} = P_{\propto} - P_{con} - P_{rad}$$

steady-state condition.

(A.1)

Where W is total stored energy.

Main input variables are geometrical parameters, plasma current, density, and temperature. At the given input value, the required heating power for each temperature density is finally calculated. It is a kind of scheme to calculate the external heating power at each density temperature domain and contour plot to

understand the driving characteristics of the demonstration and further analyze the driving path. Furthermore, depending on the curvature of the contour, it can be seen that each point is thermally stable or unstable.

The source term is alpha heating, and external heating power. Alpha heating is calculated using the Hively fusion cross section formula [38], and temperature and density are input values.

$$P_\alpha = n_D n_T < \sigma v >_{DT} E_\alpha V \qquad \text{(A.2)}$$

Loss term is composed of conduction loss and radiation loss. Conduction loss is the stored energy divided by ITER confinement time scaling [22].

$$\mathrm{P_{con}} = Stored\ Energy\ / ITER_{\tau_E} \qquad \text{(A.3)}$$

Among the radiation, impurity radiation has a relatively small influence, so we considered three dominant radiations. Each type has a temperature-sensitive or density-sensitive characteristic and a dominant regime. The higher the temperature, the more difficult it is to reach the region where cyclotron radiation and synchrotron radiation become stronger. The radiation loss formulas used are as follows.

Breamsstrahlung [39]

$$\mathrm{P_{brem}} = 4.8 \cdot 10^{-3} Z_{eff} n_e^2 \sqrt{T} a^2 R_0 \kappa \ [\mathrm{MW}] \tag{A.4}$$

ne : volume averaged density in m^{-3} T : average temperature in keV

minor radius (a) Major radius(R_0) in meter κ : the plasma elongation.

Cyclotron [40]

$$\mathrm{P_{EC}} = 4.14 \cdot 10^{-7} \frac{\sqrt{n_e^{eff}} \left(T_e^{eff}\right)^{2.5} B_T^{2.5} \sqrt{1-R_W}}{\sqrt{a_{eff}}} \left(1 + 2.5 \frac{T_e^{eff}}{511}\right) V \ [MW]$$

$$\mathrm{T_e^{eff}} = \int_0^1 T_e(\rho) d\rho \quad n_e^{eff} =< n_e > \quad \mathrm{a_{eff}} = a\sqrt{\kappa} \tag{A.5}$$

density is in $10^{20} m^{-3}$ R_W : reflection coefficient ρ : normalized minor radius

V : plasma volume in m^3.

Synchrotron [41]

$$P_{sync} = 3.84 \times 10^{-8} (1-r)^{0.5} R a^{1.38} k^{0.79} B_t^{2.62} n_{e20}^{0.38} T_e (16 + T_e)^{2.61} \left(1 + 0.12 \frac{T_e}{p_{a0}^{0.41}}\right)^{-1.51}$$

$$\times K(\alpha_n, \alpha_T, \beta_T) \quad G(A) \quad [MW]$$

$$G(A) = 0.93[1 + 0.85 \exp(-0.82A)] \qquad p_{a0} = 6.04 \times 10^3 a n_{\mathrm{e20}} / \mathrm{B_t}$$

$$K(\alpha_n + 3.87\alpha_T + 1.46)^{-0.79} (1.98 + \alpha_T)^{1.36} \beta_T^{2.14} \left(\beta_T^{1.53} + 1.87\alpha_T - 0.16\right)^{-1.33}$$

(A.6)

Using expression of J. Friedberg [42], required total heating power and confinement time could be derived

$$\sim\tau_{\mathrm{E}} \equiv K/P_{tot}^{0.69}$$

$$P_{tot} = P_{alpha} + P_{ext} - P_{rad} = \frac{W}{\tau_E}$$

$$P_{tot}^{0.31} \qquad \tau_{\mathrm{E}} \equiv K \qquad (A.7)$$

$$\left(\frac{W}{K}\right)^{\frac{1}{0.31}} \qquad \left(\frac{W}{K}\right)^{\frac{0.69}{0.31}}$$

$$P_{ext} = \left(\frac{W}{K}\right)^{\frac{1}{0.31}} - P_{alpha} + P_{rad}$$

Radiation power and stored energy is calculated from input density and temperature. Overall calculation domain is density and temperature space.

Figure A.1 and A.2 are applications for KSTAR operations and detailed parameters are in table A.1.

Table A.1. KSTAR parameters

Variable	*Value*
Major/minor radius (m)	**1.8/0.5**
Elongation	**1.8**
Z_{eff}, M	**2.3, 2**
Density and Temperature Distribution	$\boldsymbol{n(\rho) = (\alpha_N + 1)\overline{n}(1-\rho^2)^{\alpha_N}}$ $\mathbf{T(\rho) = (\alpha_T + 1)\overline{T}(1-\rho^2)^{\alpha_T}}$

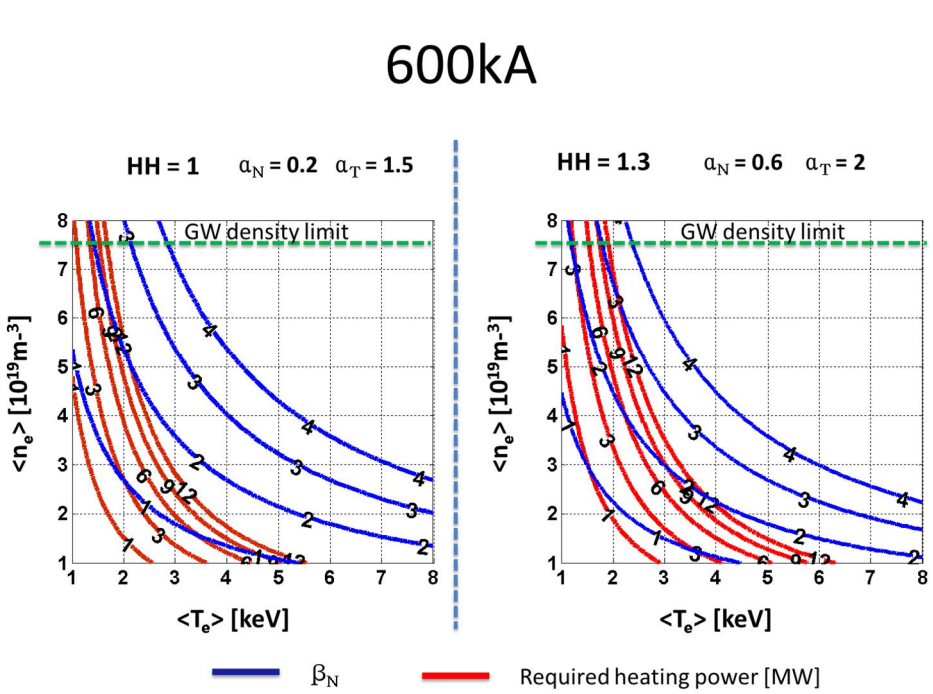

Figure A.1. KSTAR 600kA global power balance analysis.

1MA

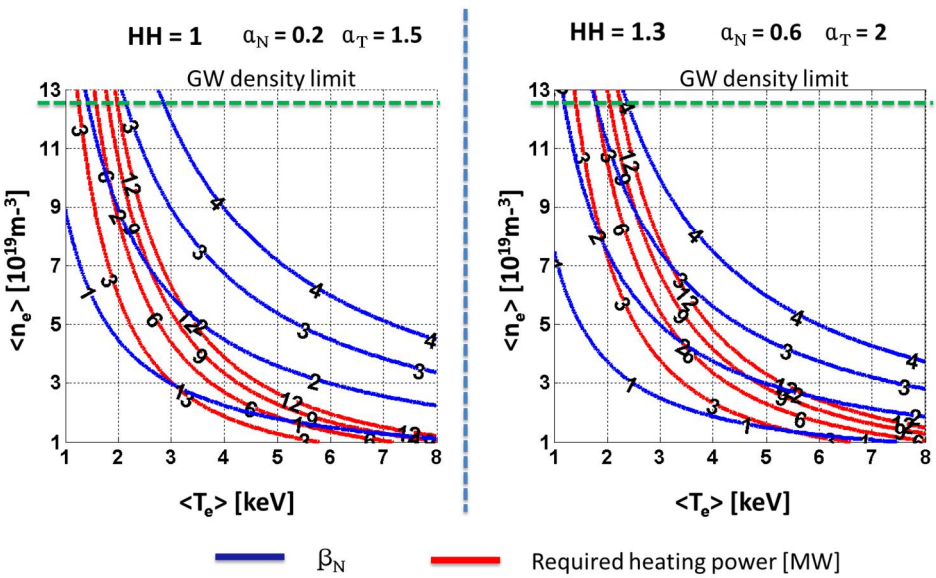

Figure A.2. KSTAR 1MA global power balance analysis.

B. Script example of code integration

Here is an actual code script of esc-IMAS connection.

```
open database

shot =20

run = 2

treename = 'ids'      ! Use standard IMAS database

time=1.d0


open(10,file='input_DB',status='old')

read(10,nml=input_p)

close(10)


call imas_open(treename,shot,run,idx) ! Opens Data Entry
```

```
  get equilibrium

  call ids_get(idx,"equilibrium",equilibrium)


call esc wrapper

  call escinimas(equilibrium,time)


put equilibrium

  call ids_put(idx,"equilibrium",equilibrium)


close database

  call ids_deallocate(equilibrium)      !! Deallocate cleanly the IDS


  call imas_close(idx) !! close the Data Entry


end program stand_alone_esc
```

C. Technological readiness of current drive method

For the selection of K-DEMO current drive method, it is essential to investigate current heating and current drive technology and their future prospect in demo operation phase. Most popular four current drive method; neutral beam, electron cyclotron wave, ion cyclotron wave, and lower hybrid wave are reviewed.

Overall current drive efficiency could be classified into three groups.

- Conversion efficiency (η_{con}): power launched by the system per electric power used to operate the system
- Coupling efficiency (η_{coup}): power coupled to the plasma per power launched
- Current drive efficiency (γ_{CD}): plasma current driven per power coupled to the plasma

So, total current drive efficiency is

$$\eta_{CD} = \eta_{conv} \times \eta_{coup} \times \gamma_{CD} \qquad (C.1)$$

The first, the conversion efficiency is determined by source and transmission line.

Neutral Beam

The most likely component of the NB source efficiency improvement is the neutralization device. At present, neutralization efficiency and transmission efficiency of positive ion beam are 35% and 70%, respectively. [43] At the phase of successful operation of ITER negative-ion beam injection system, the source efficiency is expected to increase from 35 % to 55 % [44].

In addition, transmission efficiency is expected to increase from 70 % to 90 % by using negative-ion. [45] It is theoretically predictable that a metal vapor-based neutralization device [46] or a photo-detachment-based neutralization device [47], which is expected to be completed at the end of ITER, will exhibit source and transmission efficiencies of up to 100%. However, continuous and intensive research is needed to bring this technology to reality. Therefore, the NB conversion efficiency is 55 [%] × 90 [%] = 50 [%] when viewed at ITER level.

Table C.1. NB conversion efficiency

[%]	Source (Neutralizer)	Transmission	Total
Positive Ion	**35**	**70**	**25**
Negative Ion	**55**	**90**	**50**
Metal Vapor	**65**	**100**	**65**
Photo-detachment	**100**	**100**	**100**

Electron cyclotron

Table C.2. EC conversion efficiency

[%]	Source	Others	Total
Standard Tube Gyrotrons	**40**	**(95)**	**38**
Depressed Collector Gyrotrons	**55**	**(95)**	**52.25**
Japan ITER Gyrotron	**55**	**(95)**	**52.25**

The source of the electron cyclotron resonance frequency (ECRF) is gyrotron. The most prominent part of gyrotron is the tube, and currently commercial gyrotron tubes have an efficiency of 40 % [43]. The depressed collector type gyrotron tube, which is expected to be developed at the completion of ITER, is expected to increase this efficiency to 55 % [48]. A more advanced type of multi-stage depressed collector tube is under development and expected to be 65% efficient. The efficiency of waveguide and electromagnetic wave transmission system other than gyrotron is 95 %, and there is no research field expected to improve this efficiency. Therefore, the EC conversion efficiency in the table is 55 % × 95 % = 52.25 %.

Ion cyclotron wave

Table C.3. IC conversion efficiency

[%]	Source	Others	Total
Tetrode Tubes	**70**	**(90) × 90**	**57**
Diacrode Tubes for increased power per unit			

The source of the Ion cyclotron resonance frequency (ICRF) is commercial RF power. RF power is widely used in various fields, so technical progress has been made to some extent, and tetrode tubes with efficiency of 70 % are used. [43] In the future, diacrode tubes are being studied to increase the output per unit of the IC source, which does not seem to have a significant effect on RF power efficiency. The efficiency of the system other than the source can be considered as the transmission efficiency 90 % and the high voltage power source (HVPS) efficiency 90 %. [43] Therefore, the IC conversion efficiency in the table is 70 % × 90 % × 90 % = 57 %.

Lower hybrid

Table C.4. LH conversion efficiency

[%]	Source	Others	Total
Klystrons	**46**	**88 × 90**	**36**
Klystrons with depressed collectors	**70**	**88 × 90**	**55**

Using commercially available klystron tubes, the efficiency of 46 %, which is similar to EC, can be expected. [49] However, depressed collector tubes have been studied, and 70 % efficiency is expected to be developed and expected to be completed after the ITER. [50] Transmission efficiency 88 % and high-voltage power (HVPS) efficiency 90 % are demonstrated. [43] Therefore, the LH conversion efficiency in the table is 46 % × 88 % × 90 % = 36 %.

The second, coupling issues for IC & LH.

Coupling efficiency is mainly discussed for IC and LH only. Typical coupling efficiency problems are caused by load changes at the plasma edge, and can be triggered by ELM, especially in H mode. Currently, research is underway to deal with this problem.

In the case of IC, electric power is reflected by ELM and it is input to the transmission system and it affects the power source. Experiments in JET have shown that the efficiency of the IC is reduced by a factor of three when entering the H-mode plasma, compared to entering the L-mode plasma. [51] It was confirmed that 7 MW of the 8 MW output in the ELMy H mode was coupled to the plasma by the 3 dB coupler developed for the AUG. [51] In addition, the antenna under development for ITER aims at combining 7.2 MW of 8 MW output using the frequency range of 30-55 MHz. [52] Therefore, the IC coupling efficiency listed in the table is 90 %.

For the case of LH, the power coupling of 3 MW was proved as a result of coupling experiment in 20-200 Hz ELMy H mode. [53] In this experiment, a

localized plasma environment was optimized by injecting gas into the front of the antenna, and a 15 cm retracted antenna was used. The coupling efficiencies of ICs are expected in various literature, and the LH coupling efficiency is 40 % as summarized by the most recently published ITER LH paper. [53]

Table C.5. Coupling efficiency

[%]	IC Coupling
Conventional antennae	**33**
Load variation tolerant 3[dB] coupler	**88**
Load variation tolerant ITER-like antennae	**90**
	LH Coupling
Gas injection aided, 15[cm] recessed launcher	**40**

The last, current drive efficiency in plasma.

Most of the characteristics of current drive efficiency determined by physical characteristics have been studied. Recently, a method of obtaining the current drive efficiency comparable to that of NB has been realized by optimizing the angle of incidence with respect to EC. In the ITER, EC is expected to be used more widely by this study, but this report only shows the current drive efficiency that has been demonstrated to date. The unit of this efficiency is generally [$10^{20}Am^{-2}W^{-1}$], which reflects the reduction in conversion and coupling efficiency as the tokamak radius and plasma density increase.

For the most efficient current drive, it is necessary to selectively and directly accelerate the electrons using electromagnetic fields in the RF region to increase the number of high energy tail portions in the electron distribution function. In this case, the direction of accelerating the electrons may be a direction parallel to the tokamak toroidal magnetic field or a perpendicular direction. IC and LH are

parallel and EC is vertical acceleration. In the case of NB, the current is driven by directly injecting ions with momentum in the toroidal direction instead of electromagnetic waves. Among the methods described above, the electromagnetic heating in the parallel direction using the electromagnetic waves has a small dependence on the tokamak parameters because the influence of the parallel transportation to the magnetic field on the plasma is small. On the other hand, vertical electron heating is strongly influenced by tokamak parameters, especially temperature. Therefore, IC and LH have less change of current drive efficiency according to temperature, and EC changes greatly. In the case of NB, plasma density and temperature are particularly influenced, and depending on the energy of ions injected as much as the direct ion implantation. These characteristics are summarized by the parameter dependence of global efficiency.

LH and IC do not reach the plasma center and the plasma edge, respectively. Therefore, when local efficiency is shown with respect to the radial direction of the tokamak, LH is obtained at the edge and IC is obtained at the center with the maximum value. On the other hand, EC and NB do not depend on the tokamak radial direction, and they show a flat straight line. As described above, the center current driving using the LH or the edge current driving using the IC is an unrealistic method because it shows a very low efficiency. The total current drive

efficiency considering all the radial efficiency is 50 % at 30 % based on DEMO plasma. However, EC is expected to have an efficiency of 20 % based on ITER plasma, and the current drive efficiency theory for DEMO plasma has not yet reached a global consensus but it is expected to be higher than 30 %. In the case of LH, there is little dependence on the plasma parameters, so the DEMO plasma has the lowest physical current drive efficiency, and this efficiency is inherent limit of the LH current drive method.

Table C.6. Current Drive Efficiency [54, 55]

	Global Efficiency γ [A/m^2/W]	**Parameter Dependence of Global Efficiency ξ [A/m^2/W/keV]**	**Local Efficiency Profile**
LHCD	**0.3 – 0.4**	**0**	**Peaked at edge**
ECCD	**> 0.2 (ITER parameters)**	**> 0.3 (linear)**	**Flat**

ICCD	**0.3**	**0.1 – 0.2**	**Peaked at core**
NBCD	**0.5**	**0.4 – 0.5 (linear)**	**Flat**

According to recent publication on demonstrated power from J. Pamela [43], overall efficiency is summarized in table C.6.

Table C.7. Current drive efficiencies and demonstrated power

	Conversion [%]	***Coupling [%]***	***Current Drive Efficiency [10^{20} $A/m^2/W$]***	***Overall Efficiency [10^{20} $A/m^2/W$]***	***Demonstrated Power [MW]***
NBI	**<50**	**~100**	**0.50**	**0.25**	**25**
ICRH	**<57**	**<90**	**0.40**	**0.21**	**7.2**

ECRH	**<52**	**~100**	**0.20**	**0.10**	**2.4**
LHCD	**<36**	**<40**	**0.40**	**0.06**	**3**

Bibliography

[1] K. Kim, K. Im, H.C. Kim, S. Oh, J.S. Park, S. Kwon, Y.S. Lee, J.H. Yeom, C. Lee, G-S. Lee, G. Neilson, C. Kessel, T. Brown, P. Titus, D. Mikkelsen and Y. Zhai, "Design concept of K-DEMO for near-term implementation", Nuclear Fusion 55 (2015) 053027.

[2] M. Murakami1, J.M. Park, G. Giruzzi, J. Garcia, P. Bonoli, R.V. Budny, E.J. Doyle, A. Fukuyama, N. Hayashi, M. Honda, A. Hubbard, S.Ide, F. Imbeaux, E.F. Jaeger, T.C. Luce, Y.-S. Na, T. Oikawa, T.H. Osborne, V. Parail, A.Polevoi, R. Prater, A.C.C. Sips, J. Snipes, H.E. St. John, P.B. Snyder, I. Voitsekhovitch and ITPA/Integrated Operation Scenario Group, "Integrated modelling of steady-state scenarios and heating and current drive mixes for ITER", Nuclear Fusion 51 (2011) 103006.

[3] C. E. Kessel, M. S. Tillack, F. Najmabadi, F. M. Poli, K. Ghantous, N. Gorelenkov, X. R. Wang, D. Navaei, H. H. Toudeshki, C. Koehly, L. EL-Guebaly, J. P. Blanchard, C. J. Martin, L. Mynsburge, P. Humrickhouse, M. E. Rensink, T. D. Rognlien, M. Yoda, S. I. Abdel-Khalik, M. D. Hageman, B. H. Mills, J. D. Rader, D. L. Sadowski, P. B. Snyder, H. St. John, A. D. Turnbull, L. M. Waganer, S. Malang and A. F. Rowcliffe, "THE ARIES

ADVANCED AND CONSERVATIVE TOKAMAK POWER PLANT STUDY", Fusion Science and Technology 67 (2015) 1.

[4] J. Garcia, G. Giruzzi, J.F. Artaud, V. Basiuk, J. Decker, F. Imbeaux, Y. Peysson and M. Schneider, "Analysis of DEMO scenarios with the CRONOS suite of codes", Nuclear Fusion 48 (2008) 075007.

[5] K. Tobita, S. Nishio, M. Enoeda, M. Sato, T. Isono, S. Sakurai, H. Nakamura, S. Sato, S. Suzuki, M. Ando, K. Ezato, T. Hayashi, T. Hayashi, T. Hirose, T. Inoue, Y. Kawamura, N. Koizumi, Y. Kudo, R. Kurihara, T. Kuroda, M. Matsukawa, K. Mouri, Y. Nakamura, M. Nishi, Y. Nomoto, J. Ohmori, N. Oyama, K. Sakamoto, T. Suzuki, M. Takechi, H. Tanigawa, K. Tsuchiya, D. Tsuru, "Design study of fusion DEMO plant at JAERI", Fusion. Eng. Des. 81 (2006) 1151.

[6] Feng, K. M, G.S. Zhang, G.Y. Zheng, Z. Zhao, T. Yuan, Z.Q. Li, G.Z. Sheng, C.H. Pan, "Conceptual design study of fusion DEMO plant at SWIP", Fusion. Eng. Des. 84 (2009) 2109.

[7] Arno Goedeke, Matthijs G.T. Mentink, Daniel R. Dietderich, and Andries den Ouden, "Characterization of High Current RRP Wires as a Function of

Magnetic Field, Temperature, and Strain", IEEE Trans. Appl. Supercond. 19 (2009) 2610.

[8] S. C. Jardin, C.E. Kessel, T.K. Mau, R.L. Miller, F. Najmabadi, V.S. Chan, M.S. Chu, R. LaHaye, L.L. Lao, T.W. Petrie, P. Politzer, H.E. St.John, P. Snyder, G.M. Staebler, A.D. Turnbull, W.P. West, "Physics basis for the advanced tokamak fusion power plant, ARIES-AT", Fusion Engineering and Design 80 (2006) 25.

[9] C. E. Kessel, T. K. Mau, S. C. Jardin, and F. Najmabadi, "Plasma profile and shape optimization for the advanced tokamak power plant, ARIES-AT, Fusion. Eng. Des. 80 (2006) 63-77.

[10] J. S. Kang, L. Jung, C.-S. Byun, D.H. Na, Y.-S. Na, and Y. S. Hwang., "Exploration of One-dimensional Plasma Current Density Profile for K-DEMO Steady-state Operation", Fusion. Eng. Des. 109-111, Part A (2016) 724.

[11] C. Angioni and O. Sauter, "Neoclassical transport coefficients for general axisymmetric equilibria in the banana regime", Physics of Plasmas 7 (2000) 1224.

[12] Glenn Bateman, Arnold H. Kritz, Jon E. Kinsey, Aaron J. Redd, and Jan

Weiland, “Predicting temperature and density profiles in tokamaks”, Physics of Plasmas 5 (1998) 1793.

[13] Yong-Su Na, G.D. Conway, O. Gruber, J. Hobirk, M. Maraschek, D. Nishijima, J. Schirmer, A.C.C. Sips, A. Stäbler, G. Tardini and the ASDEX Upgrade Team, “Transport studies in improved H-mode at ASDEX Upgrade”, Nuclear fusion 46 (2006) 232.

[14] Yong-Su Na, C.E. Kessel, J.M. Park, Sumin Yi, A. Becoulet, A.C.C. Sips and J.Y. Kim, “Simulations of KSTAR high performance steady state operation scenarios”, Nuclear fusion 49 (2009) 115018.

[15] S.P. Hirshman and D. J. Sigmar, “Neoclassical transport of impurities in tokamak plasmas”, Nuclear Fusion 21 (1981) 1079.

[16] M. Greenwald, J.L. Terry, S.M. Wolfe, S. Ejima, M.G. Bell, S.M. Kaye, and G. H. Neilson, “A new look at density limits in tokamaks”, Nuclear Fusion 28 (1988)

[17] W. A. Houlberg, S. E. Attenberger and L. M. Hively, “Contour analysis of fusion reactor plasma performance”, Nuclear Fusion 22 (1982).

[18] J. E. Menard, M. G. Bell, R. E. Bell, D. A. Gates, S. M. Kaye, and B. P. LeBlanc, R. Maingi, S. A. Sabbagh, D. Stutman, NSTX National Research

Team, “Aspect ratio scaling of ideal no-wall stability limits in high bootstrap fraction tokamak plasmas”, Physics of Plasma 11 No.2 (2004) 639.

[19] J. Wesson, Tokamaks second edition, Clarendon press(1997), p111

[20] C.P.C. Wong, J.C. Wesley, R.D. Stambaugh, and E.T. Cheng, “Toroidal reactor designs as a function of aspect ratio and elongation”, Nucl. Fusion 42 (2002) 547.

[21] C. Neumeyer, Y-K. Peng, C. Kessel, and P.Rutherford, “Spherical Torus Design Point Studies”, Princeton Plasma Physics Lab Report PPPL-4165 (2006).

[22] ITER Physics Expert Groups on Confinement and Transport and Confinement Modelling and Database, ITER Physics Basis Editors, “Plamsa confinement and transport”, Nuclear Fusion 39 (1999) 2175.

[23] F. Imbeaux, S.D. Pinches, J.B. Lister, Y. Buravand, T. Casper, B. Duval, B. Guillerminet, M. Hosokawa, W. Houlberg, P. Huynh, S.H. Kim, G. Manduchi, M. Owsiak, B. Palak, M. Plociennik, G. Rouault, O. Sauter and P. Strand, “Design and first applications of the ITER integrated modelling & analysis suite”, Nuclear Fusion 55 (2015) 123006.

[24] L.E. Zakharov and A. Pletzer, "Theory of perturbed equilibria for solving the Grad-Shafranov equation", Physics of Plasmas 6 (1999) 4693.

[25] H. Lutjens et al, “The CHEASE code for toroidal MHD equilibria”, Computer Physics Communications 97 (1996) 219-260.

[26] G. V. Pereverzev and P. N. Yushmanov, “ASTRA Automated System for Transport Anlaysis”, MPI fur PP Report ZB:IPP 5-98 (2002).

[27] J.E. Kinsey, G.M. Staebler, J. Candy, R.E. Waltz and R.V. Budny, “ITER predictions using the GYRO verified and experimentally validated trapped gyro-Landau fluid transport model”, Nuclear Fusion 51 (2011) 083001.

[28] MAU, T.K., et al., Radio Frequency Power in Plasmas: 13th Top. Conf., American Institue of Physics, Conf. Proc. 485, New York, 1999, p. 148.

[29] Alexei Pankin, Douglas McCune, Robert Andre, Glenn Bateman, and Arnold Kritz, “The Tokamak Monte Carlo Fast Ion Module NUBEAM in the National Transport Code Collaboration Library”, Comput. Phys. Commun. 43 (2004) 61.

[30] Glasser, A. H. and Chance, M. S., “Determination of free boundary ideal MHD stability with DCON and VACUUM”, Bulletin of the American Physical Society Vol. 42, p. 1848 (1997).

[31] A. B. Mikhailovskii, G. T. A. Huysmans, W. O. K Kerner, and S. E. Sharapov, "Optimization of Computational MHD Normal-mode Analysis for Tokamaks", Plasma physics reports, 23(10), p. 844 (1997).

[32] Luce, T. C., "Realizing steady-state tokamak operation for fusion energy", Physics of Plasmas 18 (2011) 030501.

[33] J. W. Connor, R. J. Hastie, H. R. Wilson, R. L. Miller, "Magnetohydrodynamic stability of tokamak edge plasmas", Physics of Plasmas 5 (1998) 2687.

[34] P. B. Snyder, H. R. Wilson, J. R. Ferron, L. L. Lao, A. W. Leonard, T. H. Osborne, A. D. Turnbull D. Mossessian, M. Murakami, and X. Q. Xu, "Edge localized modes and the pedestal: A model based on coupled peeling–ballooning modes", Physics of Plasmas 9 (2002) 2037.

[35] C.T. Holcomb, J.R. Ferron, T.C. Luce, T.W. Petrie, J.M. Park, F. Turco, M.A. Van Zeeland, M. Okabayashi, C.T. Lasnier, and J.M. Hanson, "Steady state scenario development with elevated minimum safety factor on DIII-D", Nuclear Fusion 54 (2014).

[36] J. M. Park, M. Murakami, C. C. Petty, W. W. Heidbrink, T. H. Osborne, C. T. Holcomb, M. A. Van Zeeland, R. Prater, T. C. Luce, M. R. Wade, M. E.

Austin, N. H. Brooks, R. V. Budny, C. D. Challis, J. C. DeBoo, J. S. deGrassie, J. R. Ferron, P. Gohil, J. Hobirk, E. M. Hollmann, R. M. Hong, A. W. Hyatt, J. Lohr, M. J. Lanctot, M. A. Makowski, D. C. McCune, P. A. Politzer, H. E. St John, T. Suzuki, W. P. West, E. A. Unterberg, and J. H. Yu, "Validation of on- and off-axis neutral beam current drive against experiment in DIII-D", Physics of Plasmas 16 (2009) 092508.

[37] M. Kuriyama, N. Akino, M. Araki, N. Ebisawa, M. Hanada, T. Inoue, M. Kawai, M. Kazawa, J. Koizumi, T. Kunieda, M. Matsuoka, K. Miyamoto, M. Mizuno, K. Mogaki, Y. Ohara, T. Ohga, Y. Okumura, H. Oohara, F. Satoh, T. Suzuki, S. Takahashi, T. Takayasu, H. Usami, K. Usui, K. Watanabe, M. Yamamoto, and T. Yamazaki, "High energy negative-ion based neutral beam injection system for JT-60U", Fusion Eng. Des. 26 (1995) 445.

[38] L.M. Hively and G.H. Miley, "Fusion product bombardment of a tokamak first wall", Nuclear Fusion 17 (1977) p873.

[39] S.C. Jardin, C.E. Kessel, D. Meade, and C. Neumeyer, "Systems Analysis of a Compact Next Step Burning Plasma Experiment", Princeton Plasma Physics Lab Report PPPL-3666 (2002).

[40] A. B. Kukushkin and P.V. Minashin, XXXVI international conference on plasma physics and CF, February 9-13, 2009, Zvenigorod.

[41] F. Albajar, J. Johner and G. Granata, "Improved calculation of synchrotron radiation losses in realistic tokamak plasmas", Nuclear fusion 41 (2001) 665.

[42] J. Friedberg, "Plasma Physics and Fusion Energy", Cambridge (2007).

[43] J. Pamela, A. Bécoulet, D. Borbaa, J.-L. Boutard, L. Horton, and D. Maisonnier, "Efficiency and availability driven R&D issues for DEMO", Fusion Eng. Des. 84 (2009) 194

[44] M. Kuriyama, N. Akino, N. Ebisawa, L. Grisham, A. Honda, T. Itoh, M. Kawai, M. Kazawa, K. Mogaki, Y. Ohara, T. Ohga, Y. Okumura, H. Oohara, N. Umeda, K. Usui, K. Watanabe, M. Yamamoto, and T. Yamamoto, "Operation and Development of the 500-keV Negative-Ion-Based Neutral Beam Injection System for JT-60U", Fusion Science and Technology 42 (2002) 410.

[45] O. Kaneko, Y. Takeiri, K. Tsumori, Y. Oka, M. Osakabe, K. Ikeda, K. Nagaoka, T. Kawamoto, E. Asano and M. Sato, "Engineering prospects of negative-ion-based neutral beam injection system from high power operation for the large helical device", Nuclear Fusion 43 (2003) 692.

[46] L. R. Grisham, “Lithium jet neutralizer to improve negative hydrogen neutral beam systems”, Physics of Plasmas 14 (2007) 102509.

[47] W. Chaibi, AIP conference proceeding negative ion beams and source conference, Aix-ex-Provence, France, 2008.

[48] A. Kasugai, K. Sakamoto, K. Takahashi, K. Kajiwara and N. Kobayash, “Steady-state operation of 170 GHz–1 MW gyrotron for ITER”, Nuclear Fusion 48 (2008) 054009.

[49] Ph. Bibet, F. Mirizzib, P. Bosiaa, L. Doceula, S. Kuzikovc, K. Rantamäkid, A.A. Tuccillob, and F. Wasasterjnad, “Overview of the ITER-FEAT LH system”, Fusion Eng. Des. 66 (2003) 525.

[50] F. Kazarian, 25th SOFT, Rostock, Germany.

[51] M. Nightingale, 22nd IAEA FEC, Geneva, Switzerland .

[52] K. Vulliez, 22nd IAEA FEC, Geneva, Switzerland.

[53] J. Hillairet, A. Ekedahl, M. Goniche, Y.S. Bae, J. Achard, A. Armitano, B. Beckett, J. Belo, G. Berger-By, J.M. Bernard, E. Corbel, L. Delpech, J. Decker, R. Dumont, D. Guilhem, G.T. Hoang, F. Kazarian, H.J. Kim, X. Litaudon, R. Magne, L. Marfisi, P. Mollard, W. Namkung, E. Nilsson, S. Park, Y. Peysson, M. Preynas, P.K. Sharma, M. Prou and the Tore Supra

Team, “Recent progress on lower hybrid current drive and implications for ITER”, Nucl. Fusion 53 (2013) 073004.

[54] H. Zohm et al, International MFE Roadmapping Workshop, Princeton, USA, 2011.

[55] D. A. Rasmussen et al, International MFE Roadmapping Workshop, Princeton, USA, 2011.

국 문 초 록

핵융합실증로 정상상태 운전을 위한 체계적이고 자기충족적인 알고리즘 개발

강 지 성
에너지시스템공학부
(핵융합 및 플라즈마 공학 전공)
서울대학교 대학원

한국의 핵융합실증로 사업은 자급 자족이 가능한 순 발전을 실현하는 것과 구성 요소 시험 시설의 목적을 가진다. KSTAR 자석의 초전도 물질 및 제조 경험의 최근 발전은 7T 이상의 플라즈마 중심에서 높은 중심 자기장을 갖는 K-DEMO의 뚜렷한 설계 특징을 이끌어 낸다.

연소 플라즈마는 대부분의 가열이 알파 입자로부터 발생하는 자체 구조 플라즈마의 일종이며 대부분의 플라즈마 전류는 현재의 실험 장치와 다른 자체 구동 전류에 의해 유지됩니다. 이러한 복잡한 현상을 계산 방법으로 분석하기 위해서는 통합된 수치 패키지가 강하게 요구되며, 체계적이고 자기-충족적 알고리즘이 필수적이다.

자석 코일 및 그 주변을 기반으로, 장/부 반경과 같은 기하학적 변수가 결정된다. 전반적인 플라즈마 성능을 평가하기 위해, 0-D 플라즈마 동작 윤곽 분석 코드가 먼저 개발되고 밀도/온도 공간에서 목표 핵융합 전력을 만족시키는 도메인 영역이 결정된다.

이 계산 체제 내에서 K-DEMO에 대한 새로운 알고리즘이 개발되어 이상적인 자기 유체 역학 (MHD) 안정성 및 기술 수준에서 정상 상태 압력 및 전류 프로파일을 처리한다. 플라즈마 감금 및 부트 스트랩 전류를 조절하는 프로파일 효과를 신중하게 고려하기 위해, 주요 변수는 최대 핵융합 증배 계수를 만드는 조건으로 압력 및 전류 밀도 프로파일로 설정된다. 서로 다른 받침대 구조를 가진 목표 압력 프로파일은 넓이, pedestal 높이 및 너비를 스캔하여 조사한다. 안정 평형의 형성은 Grad-Shafranov 방정식을 풀고 선형 MHD 안정성을 확인함으로써 평가된다. 잠재적으로 안정한 평형의 경우에 필요한 외부 가열 분포는 안정 평형의 압력 프로파일을 재현하기 위해 전력 균형과 외부 전류 드라이브 정렬을 고려하여 계산된다. 최적의 시나리오 설계를 위해 목표 융합 전력보다 높은 핵융합 증배 계수를 갖는 평형 및 해당 외부 가열 구성이 선택된다. 최종 단계로서, 전자/이온 온도 및 폴로이달 방향의 플럭스 전개는 정상 상태 시나리오를 찾고 자체 일관성있는 플라즈마 프로파일을 얻기 위해 유도 된 가열 구성으로 해결된다.

개발 된 알고리즘을 구현하기 위해 통합 수치 패키지는 표준 데이터

모델과 연결된 기존 코드로 구성된다. 이 코드 패키지는 KSTAR 결과로 벤치 마크했다.

경제적인 K-DEMO 정상 상태 목표 운영 시나리오는 평형, 안정성, 감금 및 가열 / 전류 구동과의 일관성을 고려하여 설계된 알고리즘을 통해 도출됐다. 정상 상태 솔루션은 실행 가능한 발전소 시연을 보여 주고 K-DEMO 방전의 주요 특징을 결정한다. K-DEMO는 2000 MW의 첫 번째 단계부터 시작하여 3000 MW의 두 번째 단계부터 단계별 접근 방식을 목표로 삼는다. 높은 자기장, 2000MW의 안정된 압력 및 전류 프로파일에 대한 ITER의 작업 영역 외삽. 또한 강화 된 밀도 한계 및 pedestal 압력을 가정하면 최대 3000MW의 경우도 가능할 것으로 보인다. 결론적으로, 핵융합 증배 계수를 최대화하고 K-DEMO에 적용되는 정상 상태 압력 및 전류 프로파일에 대해 연소 플라즈마 작동 시나리오를 찾기 위한 체계적이고 자기-충족적 일관된 알고리즘이 개발됐다. K-DEMO의 효율적이고 안정된 연소 플라즈마 운전은 현재의 물리/공학 수준면에서 좋은 전망을 가지고있는 것으로 보인다.

주요어: 핵융합실증로, 자기-충족 적 알고리즘, 통합 분석 코드, 정상상태 압력과 전류
학 번: 2011-30284